A&A 540, A43 (2012)
DOI: 10.1051/0004-6361/201118076

Astronomy & Astrophysics

Abell 1758N from an optical point of view: new insights on a merging cluster with diffuse radio emission

W. Boschin[1], M. Girardi[2,3], R. Barrena[4,5], and M. Nonino[3]

[1] Fundación Galileo Galilei – INAF (Telescopio Nazionale Galileo), Rambla José Ana Fernández Perez 7, 38712 Breña Baja (La Palma), Canary Islands, Spain
e-mail: boschin@tng.iac.es
[2] Dipartimento di Fisica dell'Università degli Studi di Trieste – Sezione di Astronomia, via Tiepolo 11, 34143 Trieste, Italy
[3] INAF – Osservatorio Astronomico di Trieste, via Tiepolo 11, 34143 Trieste, Italy
[4] Instituto de Astrofísica de Canarias, C/Vía Láctea s/n, 38205 La Laguna (Tenerife), Canary Islands, Spain
[5] Departamento de Astrofísica, Universidad de La Laguna, Av. del Astrofísico Francisco Sánchez s/n, 38205 La Laguna (Tenerife), Canary Islands, Spain

Received 12 September 2011 / Accepted 27 January 2012

ABSTRACT

Context. The mechanisms producing the diffuse radio emission in galaxy clusters, and in particular their connection with cluster mergers, are still debated.
Aims. We seek to explore the internal dynamics of the cluster Abell 1758N, which has been shown to host a radio halo and two relics, and is known to be a merging bimodal cluster.
Methods. Our analysis is mainly based on new redshift data for 137 galaxies acquired at the Telescopio Nazionale Galileo, only four of which have redshifts previously listed in the literature. We also used photometric data from the Sloan Digital Sky Survey and from the Canada-France-Hawaii Telescope archive. We combined galaxy velocities and positions to select 92 cluster galaxies and analyzed the internal cluster dynamics.
Results. We estimate a cluster redshift of $\langle z \rangle = 0.2782$ and quite a high line-of-sight (LOS) velocity dispersion $\sigma_V \sim 1300$ km s^{-1}. Our 2D analysis confirms the presence of a bimodal structure along the NW–SE direction. We add several pieces of information to the previous merging scenario: the two subclusters (here A1758N(NW) and A1758N(SE)) cannot be separated in the velocity analyses and we deduce a small LOS velocity difference ($\Delta V_{rf,LOS} \lesssim 300$ km s^{-1} in the cluster rest-frame). The velocity information successfully shows that A1758N is surrounded by two small groups and active galaxies infalling onto, or escaping from, the cluster. Removing the two groups, we estimate $\sigma_{V,NW} \sim 1000$ km s^{-1} and $\sigma_{V,SE} \sim 800$ km s^{-1} for A1758N(NW) and A1758N(SE), respectively. We find that Abell 1758N is a very massive cluster with a range of $M = 2{-}3 \times 10^{15}\ h_{70}^{-1}\ M_\odot$, depending on the adopted model.
Conclusions. As expected for clusters that host powerful, extended, diffuse radio emissions, Abell 1758N is a major cluster merger just forming a massive system.

Key words. galaxies: clusters: individual: Abell 1758N – galaxies: clusters: general – galaxies: kinematics and dynamics

1. Introduction

Merging processes constitute an essential ingredient of the evolution of galaxy clusters (Feretti et al. 2002b). An interesting aspect of these phenomena is the possible connection between cluster mergers and extended, diffuse radio sources: halos and relics. The synchrotron radio emission of these sources demonstrates the existence of large-scale cluster magnetic fields and of widespread relativistic particles. Cluster mergers have been proposed to provide the large amount of energy necessary for electron reacceleration to relativistic energies and for magnetic field amplification (Tribble 1993; Feretti 1999, 2002a; Sarazin 2002). Radio relics ("radio gischts" as they were called by Kempner et al. 2004), which are polarized and elongated radio sources located in the cluster peripheral regions, seem to be directly associated with merger shocks (e.g., Ensslin et al. 1998; Roettiger et al. 1999; Ensslin & Gopal-Krishna 2001; Hoeft et al. 2004). Radio halos are more likely associated with the turbulence following a cluster merger, although the precise radio formation scenario remains unclear (re-acceleration vs. hadronic models, e.g., Brunetti et al. 2009; Ensslin et al. 2011). Recent semi-analytical calculations in the framework of the turbulent re-acceleration scenario have allowed the community to derive the expectations for the statistical properties of giant radio halos, in agreement with present observations that halos are found in very massive clusters (Cassano & Brunetti 2005; Cassano et al. 2006). Alternative models have been presented in the framework of hadronic models, where the time-dependence of the magnetic fields and of the cosmic ray distributions is taken into account to explain the observational properties of both halos and (most) relics (Keshet & Loeb 2010). In these models the intracluster medium (ICM hereafter) magnetization is triggered by a merger event, in part but probably not exclusively in the wake of merger shocks. Unfortunately, one has been able to study these phenomena only recently on the basis of a sufficient statistics, i.e. a few dozen clusters hosting diffuse radio sources up to $z \sim 0.5$ (e.g., Giovannini et al. 1999; see also Giovannini & Feretti 2002; Feretti 2005; Venturi et al. 2008; Bonafede et al. 2009; Giovannini et al. 2009). It is expected that new radio telescopes will highly increase the statistics of diffuse sources (e.g., LOFAR, Cassano et al. 2010a).

From the observational point of view, there is growing evidence of the connection between diffuse radio emission and cluster mergers, since up to now diffuse radio sources have been

detected only in merging systems (see Cassano et al. 2010b). In most cases the cluster dynamical state has been derived from X-ray observations (Schuecker et al. 2001; Buote 2002; Cassano et al. 2010b). Optical data are a powerful way to investigate the presence and the dynamics of cluster mergers, too (e.g., Girardi & Biviano 2002). The spatial and kinematical analysis of member galaxies allow us to reveal and measure the amount of substructure, and to detect and analyze possible pre-merging clumps or merger remnants. This optical information is indeed complementary to the X-ray information because galaxies and the ICM react on different timescales during a merger (see, e.g., the numerical simulations by Roettiger et al. 1997). In this context, we are conducting an intensive observational and data analysis program to study the internal dynamics of clusters with diffuse radio emission by using member galaxies (DARC – Dynamical Analysis of Radio Clusters – project, see Girardi et al. 2007[1]).

During our observational program, we have conducted an intensive study of the cluster Abell 1758 (hereafter A1758). A1758 is a very rich Abell cluster having Abell richness class = 3 (Abell et al. 1989). Optically, the cluster is classified as Bautz-Morgan class III (Abell et al. 1989) and a Rood-Sastry irregular cluster "F", i.e. it has a flattened configuration (Struble & Rood 1987). While A1758 was classified as a single cluster by Abell, ROSAT images show that there are two distinct clusters (Abell 1758N and Abell 1758S, hereafter A1758N and A1758S), both highly disturbed systems, separated by approximately 2 h_{70}^{-1} Mpc along the N-S direction (Rizza et al. 1998) and both very X-ray luminous: $L_X(0.1\text{–}2.4\ \mathrm{keV}) = 11.68 \times 10^{44}\ h_{50}^{-2}\ \mathrm{erg\,s^{-1}}$ and $L_X(0.1\text{–}2.4\ \mathrm{keV}) = 7.25 \times 10^{44}\ h_{50}^{-2}\ \mathrm{erg\,s^{-1}}$ (Ebeling et al. 1998, in their cosmology) for A1758N and A1758S, respectively.

The reference X-ray study for A1758 is that of David & Kempner (2004), based on both *Chandra* and *XMM-Newton* data. According to their analysis, A1758N and A1758S do not reveal any sign of interaction between the two clusters (see also Durret et al. 2011) and their LOS recessional velocity, as measured from the X-ray spectra, is within 2100 km s^{-1}, suggesting that they likely form a gravitationally bound system. Moreover, David & Kempner (2004) found that A1758N is in the late stages of a large impact parameter merger between two hot ($kT_X \sim 7$ keV) subclusters (NW and SE subclumps), with the two remnant cores separated in projection by 800 h_{70}^{-1} kpc and surrounded by hotter gas ($kT_X \sim$ 9–12 keV) that was probably shock-heated during the early stages of the merger. In particular, the *Chandra* image suggests that the X-ray NW subclump is currently moving toward the N, while the X-ray SE subclump is moving toward the SE.

The optical luminosity distribution of the cluster red-sequence galaxies reveals two luminous NW and SE subclumps, too (see Okabe & Umetsu 2008). However, while the peak position of the X-ray NW subclump coincides with that of the luminous brightest cluster member lying at NW, the X-ray SE subclump is offset by about 290 h_{70}^{-1} kpc to the NW of the optical SE structure. The bimodal feature of A1758N in the weak-lensing mass maps reported by Dahle et al. (2002) and Okabe & Umetsu (2008) shows that the mass and light are similarly distributed in A1758N. Both studies found arc candidates around the two mass peaks. The SE structure in the mass/galaxy map is located in front of the X-ray SE subclump and moves toward the south-east, while the NW structure shows no significant offset among the galaxy, ICM, and mass distributions (Okabe & Umetsu 2008; Ragozzine et al. 2012).

[1] See also the web site of the DARC project http://adlibitum.oat.ts.astro.it/girardi/darc

More recently, Durret et al. (2011) confirmed the complex structure of A1758N and the high core X-ray temperature (6–7 keV) with *XMM-Newton* data. They also found two elongated regions of high metallicity in A1758N, likely left by ram-pressure stripping during the merger of two subclusters. Moreover, using Canada-France-Hawaii Telescope (CFHT) images, Durret et al. (2011) computed A1758N and A1758S luminosity functions and discussed differences from a Schechter function in the view of the cluster internal dynamics.

As for the diffuse radio emission, the first evidence of a diffuse radio source in A1758N came from Kempner & Sarazin (2001). Giovannini et al. (2006) first reported the clear detection of a radio halo in the center of the cluster. More recently, Giovannini et al. (2009) identified a central diffuse radio emission (halo), 0.63 h_{70}^{-1} Mpc in size, and two brighter peripheral structures on the opposite sides with respect to the cluster center that resemble relic radio sources (see their Fig. 7 and our Fig. 1 for a multiwavelength view of the cluster). A1758N is one of the very few clusters with a central halo and two peripheral relics similar to RXCJ1314.4-2515 (see Feretti et al. 2005).

Spitzer/MIPS 24 μm observations of A1758 show a very active star formation in the A1758N galaxies, suggesting that dust-obscured activity in clusters is triggered by the details of cluster-cluster mergers, too (Haines et al. 2009).

To date, only a small amount of redshift data have been available for A1758; they indicate a value of $z \sim 0.28$. No internal dynamical analysis based on member galaxies has been published.

Our new spectroscopic data for A1758N come from the Telescopio Nazionale Galileo (TNG). Our present analysis is also based on public optical photometric data from the Sloan Digital Sky Survey (SDSS) and the CFHT archive.

This paper is organized as follows. We present our new optical data and the cluster catalog in Sect. 2. We present our results about the cluster structure in Sect. 3. We briefly discuss our results and present our conclusions in Sect. 4.

Unless otherwise stated, we indicate errors at the 68% confidence level (hereafter c.l.). Throughout this paper, we use $H_0 = 70$ km s^{-1} Mpc^{-1} in a flat cosmology with $\Omega_0 = 0.3$ and $\Omega_\Lambda = 0.7$. In the adopted cosmology, 1′ corresponds to $\sim$254 h_{70}^{-1} kpc at the cluster redshift.

2. Redshift data and galaxy catalog

Multi-object spectroscopic observations of A1758N were carried out at the TNG, a 4m-class telescope, in May 2008 and May 2009. We used DOLORES/MOS with the LR-B Grism 1, yielding a dispersion of 187 Å/mm. The detector is a 2048 × 2048 pixels E2V CCD, with a pixel size of 13.5 μm. In total, we observed four MOS masks (one in 2008 and three in 2009) for a total of 146 slits. The targets were chosen within the pre-imaged area (a rectangle of $\sim 8.6' \times 13.7'$ centered on the cluster and with the major side clockwise rotated by 40°) after a rough color preselection. We acquired three exposures of 1800 s for each mask. Wavelength calibration was performed using helium+argon and helium+mercury+neon lamps. Reduction of spectroscopic data was carried out using the IRAF[2] package. Radial velocities were determined using the cross-correlation technique (Tonry & Davis 1979) that is implemented in the RVSAO package (developed at the Smithsonian Astrophysical Observatory Telescope

[2] IRAF is distributed by the National Optical Astronomy Observatories, which are operated by the Association of Universities for Research in Astronomy, Inc., under cooperative agreement with the National Science Foundation.

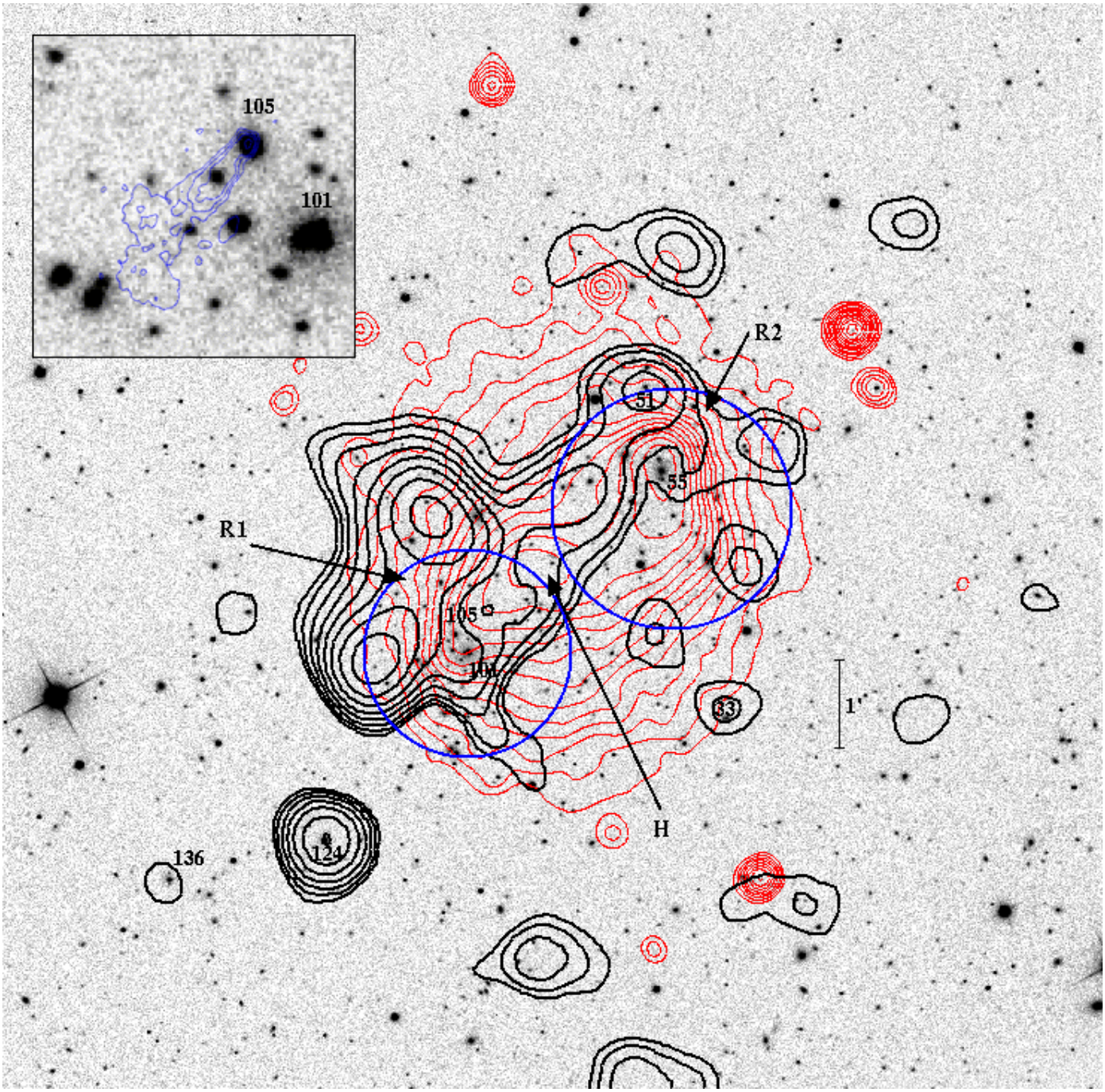

Fig. 1. Multiwavelength picture of the cluster A1758N (north at the top and east to the left). Optical density peaks detected from our analysis of the galaxy distribution (big blue circles; see Sect. 3.4) are superimposed on the SDSS r'-band image of the cluster region. Labels indicate the IDs of galaxies cited in the text. Thin red contour levels show the ICM distribution we derived from the X-ray Chandra archival image ID 2213 (photons in the energy range 0.3–7 keV; see David & Kempner 2004, for an extensive analysis of these X-ray data). From Giovannini et al. (2009) we also reproduce the radio contour levels of their VLA radio image at 1.4 GHz (thick black contours, HPBW = $45'' \times 45''$) and highlight with arrows the positions of the radio halo (H, in the center) and the two peripheral radio relics (R1 and R2). The insert on the top left is a zoom on the region of the NAT radio galaxy 1330+507 (ID 105), with the radio contours taken from VLA high-resolution radio images presented by O'Dea & Owen (1985).

Data Center). Each spectrum was correlated against six templates for a variety of galaxy spectral types: E, S0, Sa, Sb, Sc, and Ir (Kennicutt 1992). The template producing the highest value of $\mathcal{R}$, i.e., the parameter given by RVSAO and related to the signal-to-noise ratio of the correlation peak, was chosen. Moreover, all spectra and their best correlation functions were examined visually to verify the redshift determination.

In eleven cases (IDs. 1, 6, 14, 31, 48, 49, 89, 110, 113, 122 and 131; see Table 1), we had to rely on the EMSAO package to obtain an estimate of the redshift.

The formal errors as given by the cross-correlation are known to be smaller than the true errors (e.g., Malumuth et al. 1992; Bardelli et al. 1994; Ellingson & Yee 1994; Quintana et al. 2000). Duplicate observations for the same galaxy allowed us

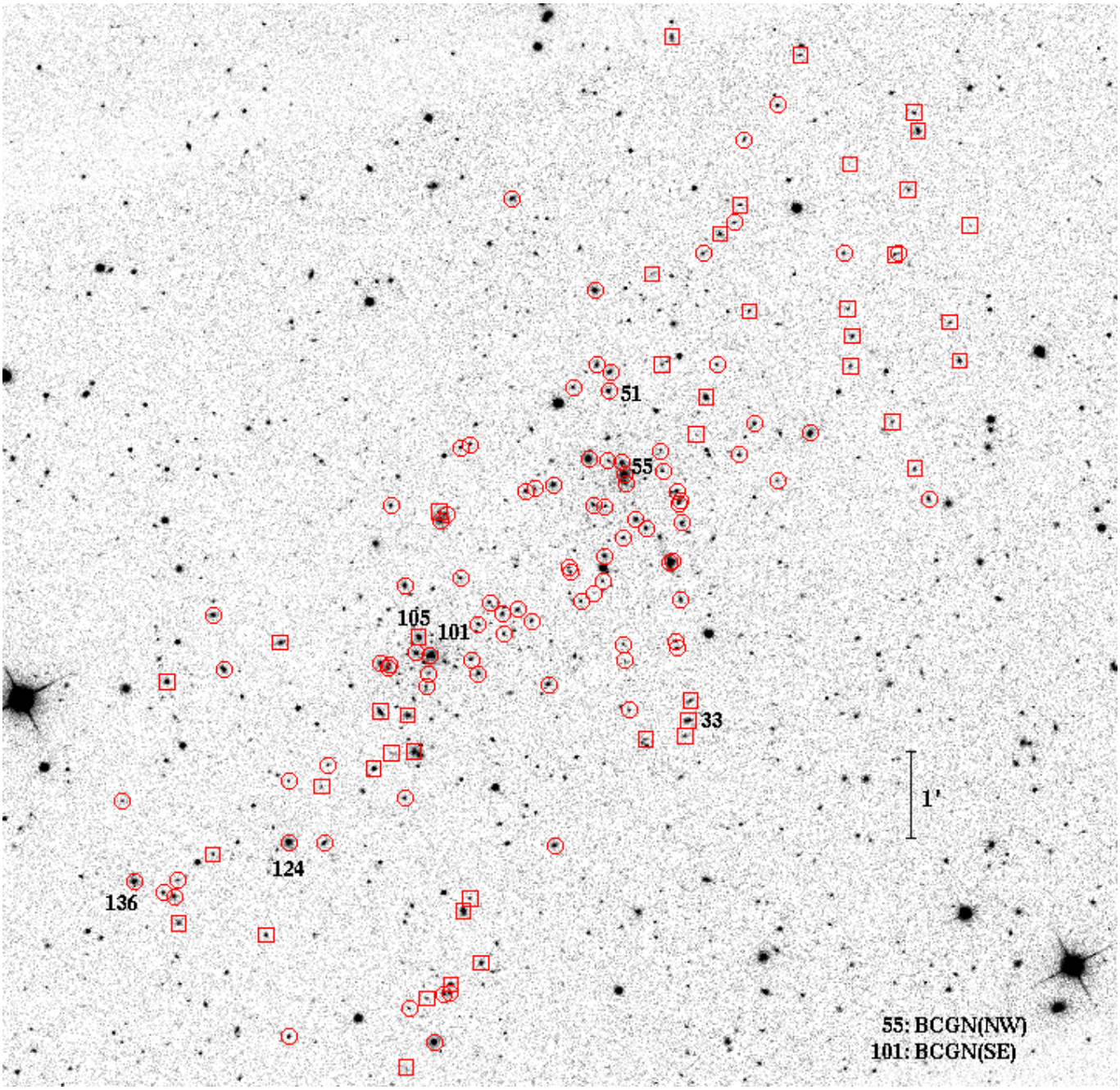

Fig. 2. SDSS r'-band image of A1758N (north at the top and east to the left) showing galaxies with measured spectroscopic redshifts. Circles and boxes indicate cluster members and nonmember galaxies, respectively (see Table 1). Labels indicate the IDs of galaxies cited in the text.

to estimate the true intrinsic errors in data of the same quality taken with the same instrument (e.g. Barrena et al. 2009). Here we have double determinations for six galaxies, therefore we decided to apply the procedure already applied in Barrena et al. (2009), obtaining that true errors are larger than formal cross-correlation errors by a factor of 2.2. For the galaxies with two redshift estimates, we used the mean of the two measurements and the corresponding errors. As for the radial velocities estimated through EMSAO we assumed the largest between the formal error and 100 km s^{-1}.

Our spectroscopic catalog lists 137 galaxies in the field of A1758N (see Fig. 2). The median error in cz is 76 km s^{-1}.

Out of 137 galaxies, only four have a previously measured redshift as listed by NED. In particular, we looked at SDSS spectroscopic data (Data Release 7) finding eight "likely" member galaxies with measured spectroscopic redshift in the field we sampled with the TNG. Out of these, only three galaxies are in common with our sample. The three redshifts agree with our estimates within 1–2σ and the difference $v_{\rm our} - v_{\rm SDSS}$ ranges between 72–92 km s^{-1} for all three galaxies. Owing to the small improvement we decided to not add the other five, preferring to work with a homogeneous sample. However, in our discussions we also consider the BCG of A1758S (RA = $13^{\rm h}32^{\rm m}32\overset{\rm s}{.}96$ and Dec = +50°25′02.5″ – J2000.0, cz = 81802 ± 52, r' = 17.13; hereafter BCGS).

We used public photometric data from the SDSS (Data Release 7). In particular, we used g', r', and i' magnitudes, already corrected for the Galactic extinction, and considered galaxies within a radius of 25′ from the cluster center.

Table 1. Velocity catalog of 137 spectroscopically measured galaxies in the field of the cluster A1758N.

ID	IDm	α, δ (J2000)	r'	v (km s^{-1})	Δv
1	–	13 32 13.95, +50 36 23.2	21.75	125 775	71
2	–	13 32 14.70, +50 34 52.4	19.65	99 042	82
3	–	13 32 15.38, +50 35 18.1	20.01	85 168	104
4	1	13 32 16.88, +50 33 19.3	19.79	80 993	94
5	–	13 32 17.62, +50 37 27.2	19.11	41 801	173
6	–	13 32 17.85, +50 33 39.6	20.10	32 788	100
7	–	13 32 17.92, +50 37 39.5	20.18	88 373	128
8	–	13 32 18.32, +50 36 47.6	20.23	98 217	93
9	2	13 32 18.98, +50 36 04.4	21.70	84 170	129
10	–	13 32 19.28, +50 36 03.8	20.21	85 959	128
11	–	13 32 19.45, +50 34 11.1	20.31	112 194	60
12	–	13 32 22.27, +50 35 08.9	19.89	98 001	50
13	–	13 32 22.42, +50 34 48.9	19.90	97 790	69
14	–	13 32 22.47, +50 37 04.5	21.95	97 872	100
15	–	13 32 22.59, +50 35 27.4	20.17	98 137	88
16	3	13 32 22.89, +50 36 04.7	20.36	84 969	60
17	4	13 32 25.27, +50 34 03.5	18.32	82 720	48
18	–	13 32 25.98, +50 38 18.2	20.16	85 091	114
19	5	13 32 27.59, +50 33 31.4	20.41	84 801	98
20	6	13 32 27.59, +50 37 44.5	19.84	82 907	92
21	7	13 32 29.23, +50 34 10.0	19.73	83 370	92
22	–	13 32 29.57, +50 35 25.8	20.33	74 891	116
23	8	13 32 29.93, +50 37 21.5	20.00	82 044	54
24	–	13 32 30.23, +50 36 37.1	20.32	113 677	79
25	9	13 32 30.27, +50 33 49.0	19.89	82 680	70
26	10	13 32 30.62, +50 36 25.5	20.04	82 111	66
27	–	13 32 31.64, +50 36 17.7	19.73	98 544	76
28	11	13 32 31.88, +50 34 49.9	20.37	83 238	123
29	–	13 32 32.64, +50 34 27.9	18.55	53 251	53
30	12	13 32 32.86, +50 36 04.5	19.96	85 335	62
31	–	13 32 33.31, +50 34 02.5	21.70	187 664	100
32	–	13 32 33.72, +50 31 03.4	19.90	112 311	98
33	–	13 32 33.86, +50 30 50.0	19.01	112 310	75
34	–	13 32 34.12, +50 30 39.7	20.22	113 091	116
35	13	13 32 34.31, +50 33 03.1	19.47	87 495	50
36	14	13 32 34.41, +50 32 11.3	19.78	80 234	41
37	15	13 32 34.49, +50 33 18.5	19.11	84 766	70
38	16	13 32 34.57, +50 33 16.2	21.48	83 263	223
39	17	13 32 34.69, +50 31 39.1	20.45	84 767	92
40	18	13 32 34.70, +50 33 24.7	19.43	81 303	72
41	19	13 32 34.75, +50 31 43.3	20.46	86 327	79
42	20	13 32 34.96, +50 32 37.3	18.75	84 194	44
43	–	13 32 35.07, +50 38 30.5	19.68	98 294	119
44	21	13 32 35.21, +50 32 36.2	18.25	81 900	71
45	22	13 32 35.69, +50 33 38.1	20.29	83 293	54
46	–	13 32 35.73, +50 34 49.8	20.83	113 693	82
47	23	13 32 35.84, +50 33 52.0	20.50	83 709	76
48	–	13 32 36.46, +50 35 50.6	20.43	87 368	100
49	–	13 32 36.88, +50 30 37.7	20.50	112 681	100
50	24	13 32 36.89, +50 32 59.7	19.54	83 963	63
51	25	13 32 37.58, +50 33 05.7	19.35	82 279	44
52	26	13 32 38.04, +50 30 57.2	20.58	84 344	79
53	27	13 32 38.33, +50 31 30.3	20.92	86 862	255
54	28	13 32 38.33, +50 33 30.1	20.48	84 176	120
55	†29	13 32 38.41, +50 33 35.7	17.15	83 489	57
56	30	13 32 38.46, +50 31 41.4	20.59	85 204	113
57	31	13 32 38.48, +50 32 53.0	20.14	83 376	76
58	32	13 32 38.58, +50 33 43.9	19.52	83 791	79
59	33	13 32 39.43, +50 34 45.0	18.97	83 208	50
60	34	13 32 39.54, +50 33 45.0	20.13	83 880	76
61	35	13 32 39.54, +50 34 32.0	19.01	87 769	85
62	36	13 32 39.76, +50 33 14.4	20.40	82 872	128
63	37	13 32 39.80, +50 32 41.0	19.37	83 803	84
64	38	13 32 39.94, +50 32 23.9	20.94	83 497	172
65	39	13 32 40.35, +50 34 49.4	19.50	85 818	70
66	40	13 32 40.51, +50 35 39.6	18.56	81 400	47
67	41	13 32 40.52, +50 32 16.0	21.97	85 932	182
68	42	13 32 40.59, +50 33 15.4	19.63	80 255	54
69	43	13 32 40.96, +50 33 46.3	17.93	83 667	38
70	44	13 32 41.47, +50 32 10.7	20.38	80 544	57
71	45	13 32 42.03, +50 34 34.7	20.19	87 429	132
72	46	13 32 42.21, +50 32 30.1	20.56	82 939	85
73	47	13 32 42.35, +50 32 33.1	20.94	81 072	91
74	48	13 32 43.30, +50 29 26.2	18.99	82 769	63
75	49	13 32 43.43, +50 33 28.8	18.80	85 478	60
76	50	13 32 43.77, +50 31 14.6	19.35	83 504	50
77	51	13 32 44.77, +50 33 26.0	19.78	84 664	97
78	52	13 32 44.96, +50 31 57.2	20.03	84 337	82
79	53	13 32 45.35, +50 33 24.6	19.47	85 798	82
80	54	13 32 45.94, +50 32 04.7	19.50	79 995	76
81	55	13 32 46.36, +50 36 41.5	18.88	86 035	47
82	56	13 32 46.90, +50 31 48.5	20.48	83 825	113
83	57	13 32 47.00, +50 32 02.0	19.77	84 249	76
84	58	13 32 47.92, +50 32 09.6	20.03	82 909	82
85	–	13 32 48.47, +50 28 06.7	19.29	109 410	85
86	59	13 32 48.71, +50 31 54.9	19.94	82 757	63
87	60	13 32 48.72, +50 31 21.7	19.47	83 562	63
88	61	13 32 49.25, +50 31 31.1	19.89	82 110	88
89	–	13 32 49.28, +50 28 50.3	20.45	161 829	100
90	62	13 32 49.32, +50 33 55.9	19.95	79 788	76
91	–	13 32 49.73, +50 28 41.6	18.64	55 954	60
92	63	13 32 50.00, +50 32 26.0	19.98	84 288	79
93	64	13 32 50.03, +50 33 53.8	20.40	81 273	60
94	–	13 32 50.62, +50 27 52.3	19.49	80 403	72
95	65	13 32 50.72, +50 27 46.7	19.55	82 691	79
96	66	13 32 51.01, +50 33 08.8	19.89	84 526	79
97	67	13 32 51.10, +50 27 45.8	19.70	81 557	82
98	68	13 32 51.42, +50 33 04.7	17.95	85 536	57
99	–	13 32 51.50, +50 33 10.3	20.16	130 803	148
100	69	13 32 51.79, +50 27 13.5	18.01	83 197	54
101	‡70	13 32 52.10, +50 31 34.1	17.02	83 864	70
102	71	13 32 52.21, +50 31 21.8	20.36	83 139	72
103	–	13 32 52.33, +50 27 42.8	20.60	109 756	204
104	72	13 32 52.41, +50 31 12.8	20.23	82 717	75
105	–	13 32 52.93, +50 31 46.1	18.52	79 682	41
106	73	13 32 53.10, +50 31 35.5	19.64	83 648	63
107	–	13 32 53.24, +50 30 29.0	18.69	99 000	47
108	74	13 32 53.57, +50 27 36.0	20.42	83 346	94
109	–	13 32 53.69, +50 30 53.3	19.06	98 877	104
110	–	13 32 53.75, +50 26 56.2	20.81	212 245	100
111	75	13 32 53.92, +50 29 57.7	19.90	82 041	66
112	76	13 32 53.94, +50 32 20.7	19.13	79 836	47
113	–	13 32 54.86, +50 30 27.8	20.89	52 848	100
114	77	13 32 54.94, +50 33 14.7	19.82	79 373	54
115	78	13 32 55.00, +50 31 27.6	21.38	84 114	154
116	79	13 32 55.15, +50 31 25.4	18.85	85 175	72
117	80	13 32 55.61, +50 31 28.5	19.01	85 239	47
118	–	13 32 55.64, +50 30 55.8	18.83	55 708	98
119	–	13 32 56.08, +50 30 17.5	18.98	31 474	70
120	81	13 32 59.32, +50 30 19.9	20.66	83 353	230
121	82	13 32 59.59, +50 29 27.6	19.24	82 055	50
122	–	13 32 59.75, +50 30 05.4	20.61	86 250	100
123	83	13 33 02.05, +50 27 17.1	19.84	82 098	54
124	84	13 33 02.07, +50 29 28.0	17.92	83 651	47
125	85	13 33 02.12, +50 30 09.2	20.88	83 434	76
126	–	13 33 02.71, +50 31 42.3	18.87	80 377	82
127	–	13 33 03.67, +50 28 25.3	19.87	93 943	91
128	86	13 33 06.72, +50 31 24.1	18.62	85 598	47
129	–	13 33 07.43, +50 29 19.6	20.35	82 058	62

Table 1. continued.

ID	IDm	α, δ (J2000)	r'	v (km s^{-1})	Δv
130	87	13 33 07.48, +50 32 00.7	18.93	82 508	47
131	–	13 33 09.83, +50 28 33.2	19.57	87 007	100
132	88	13 33 09.90, +50 29 02.3	19.94	83 139	76
133	89	13 33 10.19, +50 28 51.3	18.92	82 496	72
134	–	13 33 10.72, +50 31 15.6	18.87	86 227	40
135	90	13 33 10.93, +50 28 53.7	19.90	82 857	91
136	91	13 33 12.99, +50 29 01.3	18.52	82 798	41
137	92	13 33 13.84, +50 29 55.3	20.77	83 782	94

Notes. †, ‡ Highlight the IDs of the BCGN(NW) and BCGN(SE), respectively.

Table 1 lists the velocity catalog (see also Fig. 2): identification number of each galaxy and members, ID and IDm (Cols. 1 and 2, respectively); right ascension and declination, α and δ (J2000, Col. 3); r' SDSS magnitude (Col. 4); heliocentric radial velocities, $v = cz_\odot$ (Col. 5) with errors, Δv (Col. 6).

We also used public photometric data from the CFHT archive taken with the Megaprime/Megacam camera. We retrieved from the CADC Megapipe archive (Gwyn 2009) the catalogs for the images in the $g^{\rm Mega}$ and $r^{\rm Mega}$ bands[3] and corrected the magnitudes for the Galactic extinction. The total area covered by the images was 1.05×1.16 deg^2. The estimated limiting magnitudes (at the 5σ c.l.) are $g^{\rm Mega} = 27.0$ and $r^{\rm Mega} = 26.8$.

No evident unique dominant galaxy is present in A1758N, instead there are two BCGs: one in the NW subcluster (ID. 55, $r' = 17.15$, hereafter BCGN(NW)) and one in the SE subcluster (ID. 101, $r' = 17.02$, hereafter BCGN(SE)). They are separated by $\sim$0.85 h_{70}^{-1} Mpc and are $\sim$0.8 mag brighter than other bright galaxies in our sample. Moreover, Durret et al. (2011) found that they are characterized by a surface brightness profile flatter than those of other bright galaxies and suggested that the two BCGs are really dominant galaxies in their respective subcluster.

2.1. Radio and X-ray emitting galaxies in the field of A1758N

Our spectroscopic catalog lists some radio galaxies observed in the sky region of A1758N. At $\sim$14″ NE of BCGN(SE) we identify the galaxy ID 105 with the radio source 1330+507 (O'Dea & Owen 1985, see our Fig. 1), one of the most powerful narrow-angle tail (NAT) radio sources known with the tail pointing to the SE. Rizza et al. (2003) used high-resolution VLA data to list a total of 11 radio sources in the field of A1758, some of them members of A1758N. Interestingly, source #1 of Rizza et al. (see their Table 3) is our ID 55 (the BCGN(NW)). Other radio sources are ID 51 (#2 of Rizza et al.), ID 33 (#3, background galaxy), ID 124 (#6, the third-brightest galaxy in our spectroscopic sample) and ID 136 (#10).

According to Hart et al. (2009), BCGN(NW) is also a pointlike X-ray source. A look at the original (non-smoothed) *Chandra* X-ray image reveals that ID 124 is a faint X-ray source, too.

3. Analysis of the spectroscopic sample

3.1. Member selection

To select cluster members among the 137 galaxies with redshifts, we followed a two-step procedure. We first used the 1D adaptive-kernel method (hereafter DEDICA, Pisani 1993, 1996; see also Fadda et al. 1996; Girardi et al. 1996). We searched for significant peaks in the velocity distribution at >99% c.l. This procedure detects A1758N as a peak at $z \sim 0.278$ populated by 104 galaxies considered as candidate cluster members (in the range $79\,373 \le v \le 88\,373$ km s^{-1}, see Fig. 3). Out of 33 non-members, 8/25 are foreground/background galaxies.

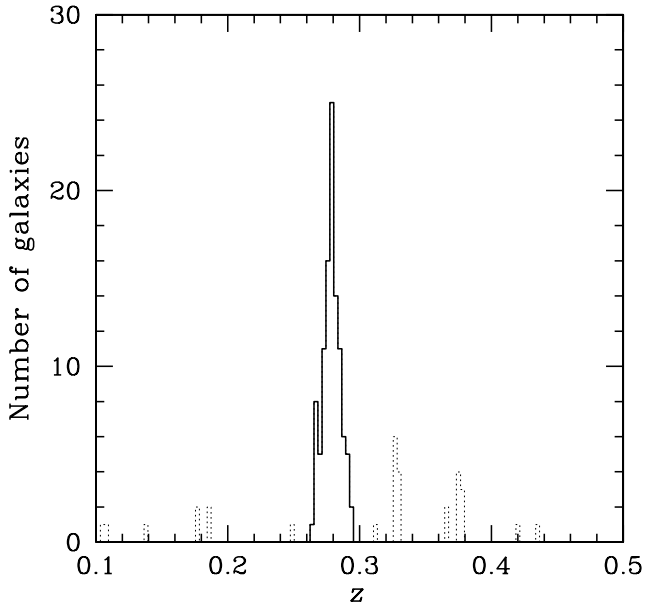

Fig. 3. Redshift galaxy distribution. The solid line histogram refers to the 104 galaxies assigned to A1758N according to the DEDICA reconstruction method.

All galaxies assigned to the cluster peak were analyzed in the second step, which combines position and velocity information, i.e., the "shifting gapper" method by Fadda et al. (1996). This procedure rejects galaxies that are too far in velocity from the main body of galaxies within a fixed bin that shifts along the distance from the cluster center. The procedure is iterated until the number of cluster members converges on a stable value. Following Fadda et al. (1996), we used a gap of 1000 km s^{-1} – in the cluster rest-frame – and a bin of 0.6 h_{70}^{-1} Mpc, or large enough to include 15 galaxies. For the center of A1758N we adopted the position of the BCGN(NW) [RA = $13^{\rm h}32^{\rm m}38\overset{\rm s}{.}41$, Dec = +50°33′35.7″ (J2000.0)]. We selected this center because, contrary to the SE subcluster, the peak position of the X-ray NW subclump coincides with that of the BCGN(NW). Moreover, the NW subcluster is more luminous, massive, and hot than the SE subcluster (Okabe et al. 2008; Durret et al. 2011), which suggests that it is the primary component of A1758N. The "shifting gapper" procedure rejected another 12 interlopers. Most of them are not very far from the main body, but we are confident enough in our rejection because 6 out of 12 are emission line galaxies (ELGs hereafter), which increases their probability of belonging to the field or to the infalling cluster region (see Sect. 4.1 for a more detailed discussion on these ELGs). Finally, we obtained a sample of 92 fiducial cluster members (see Fig. 4). The removed interlopers are shown in Fig. 5 (top panel).

3.2. General cluster properties

By applying the biweight estimator to the 92 cluster members (Beers et al. 1990, ROSTAT software), we computed a mean cluster redshift of $\langle z \rangle = 0.2782 \pm 0.0005$, i.e. $\langle v \rangle = (83390 \pm 139)$ km s^{-1}. We estimated the LOS velocity dispersion, $\sigma_{\rm V}$, by

[3] For a comparison between Megacam and SDSS filters, check the web page http://www2.cadc-ccda.hia-iha.nrc-cnrc.gc.ca/megapipe/docs/filters.html

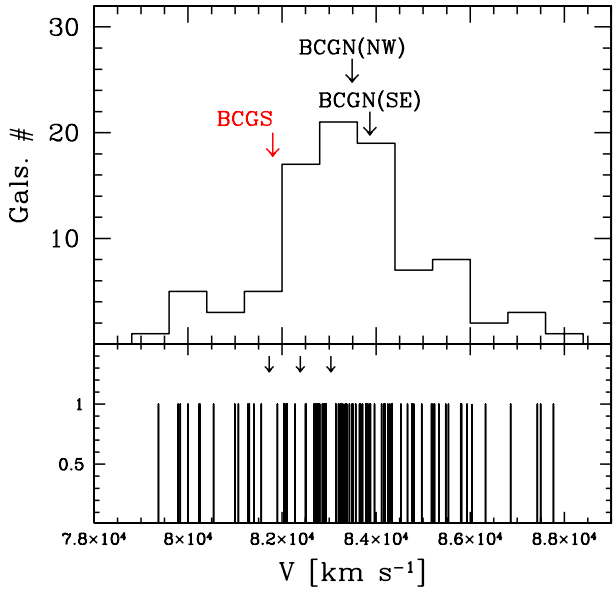

Fig. 4. The 92 galaxies assigned to the cluster A1758N. *Upper panel*: Galaxy velocity distribution. The arrows indicate the velocities of the BCGN(NW) and BCGN(SE). We also show the velocity of BCGS of A1758S as taken from the SDSS. *Lower panel*: stripe density plot where the arrows indicate the positions of the significant gaps.

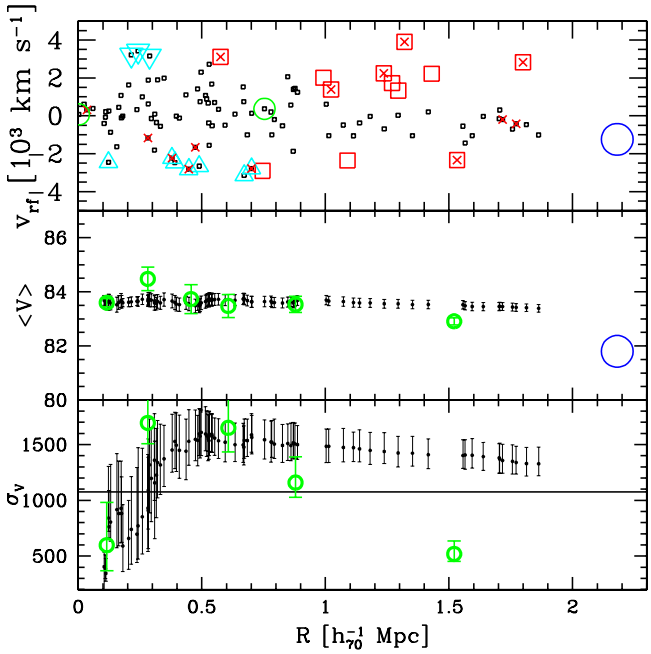

Fig. 5. *Top panel:* rest-frame velocity vs. projected distance from the cluster center (here the BCGN(NW)). Small/black and large/red squares indicate the member galaxies and those rejected as interlopers by the shifting gapper procedure, respectively. Red crosses indicate ELGs. The two green circles indicate the BCGN(NW) and the BCGN(SE). The large/blue circle indicates the BCG of A1758S using the SDSS redshift. The cyan triangles and rotated triangles indicate galaxies detected as members of HT2 and HT12 subclusters detected through the Htree-method (see Sect. 3.5). *Middle and bottom panels:* differential (big circles) and integral (small points) profiles of mean velocity and LOS velocity dispersion, respectively. For the differential profiles, we plot the values for six annuli from the center of the cluster, each containing 15 galaxies (large green symbols). For the integral profiles, the mean and dispersion at a given (projected) radius from the cluster-center is estimated by considering all galaxies within that radius – the first value computed on the five galaxies closest to the center. The error bands at the 68% c.l. are also shown. In the lower panel, the horizontal line represents the X-ray temperature (7 keV) estimated from David & Kempner (2004) for the core of the two subclusters, see also Durret et al. (2011), transformed to σ_V assuming the density-energy equipartition between ICM and galaxies, i.e. $\beta_{spec} = 1$ (see Sect. 4).

using the biweight estimator and applying the cosmological correction and the standard correction for velocity errors (Danese et al. 1980). We obtained $\sigma_V = 1329^{+135}_{-116}$ km s^{-1}, where errors are estimated through a bootstrap technique.

To evaluate the robustness of the σ_V estimate, we analyzed the velocity dispersion profile (Fig. 5). The integral profile flattens in the external cluster regions, as found for most nearby clusters (e.g., Fadda et al. 1996; Girardi et al. 1996). The sharp rising of the integral and differential profiles in the internal region is discussed in Sect. 4.1.

3.3. Velocity distribution

We analyzed the velocity distribution to search for possible deviations from Gaussianity that might provide important signatures of complex dynamics. For the following tests, the null hypothesis is that the velocity distribution is a single Gaussian.

We estimated three shape estimators, i.e., the kurtosis, the skewness, and the scaled tail index STI. We found STI = 1.294, i.e. that the velocity distribution departs from Gaussianity at the 95–99% c.l. (according to Table 1 of Bird & Beers 1993). The velocity distribution thus shows evidence for a heavy tailed distribution.

We then investigated the gaps in the velocity distribution. We followed the weighted gap analysis presented by Beers et al. (1991, 1992; ROSTAT software). We looked for normalized gaps larger than 2.25, since in random draws of a Gaussian distribution they arise at most in about 3% of the cases, independent of the sample size (Wainer & Schacht 1978). We detected three significant gaps (at the 97%, 97%, and 98.6% c.ls), which divide the cluster into four groups of 13, 9, 14, and 56 galaxies from low to high velocities (hereafter GV1, GV2, GV3, and GV4, see Fig. 4). Both BCGN(NW) and BCGN(SE) were assigned to the GV4 peak.

Following Ashman et al. (1994), we also applied the Kaye's mixture model (KMM) algorithm. We found that a partition of 13, 7, 41, and 31 galaxies is a significantly more accurate description of the galaxy distribution than a single Gaussian (at the ~97% c.l.).

3.4. Analysis of the 2D galaxy distribution

By applying the 2D adaptive-kernel method (2D-DEDICA) to the positions of the 92 member galaxies we found that the cluster is elongated in the SE-NW direction. In particular, we detected three peaks with high statistical significance: the main peak, which is coincident with the BCGN(NW), a secondary peak coincident with the BCGN(SE), and a third one, which is intermediate (Fig. 6).

Our spectroscopic data do not cover the entire cluster field and are affected by magnitude incompleteness. More precisely, we found the spectroscopic catalog has a ~50% completeness for $r' < 19$ and the completeness level quickly drops to <30% for $r' > 21$. To overcome these problems, we used the SDSS and CFHT photometric data samples, which cover a larger spatial region. The SDSS sample has the advantage to have photometry

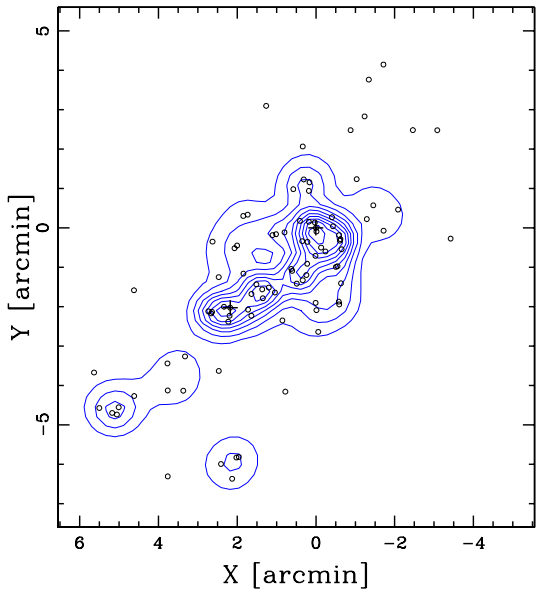

Fig. 6. Spatial distribution on the sky and relative isodensity contour map of the 92 spectroscopic cluster members, obtained with the 2D-DEDICA method. The BCGN(NW) is taken as the cluster center. Crosses indicate the location of the BCGN(NW) and BCGN(SE).

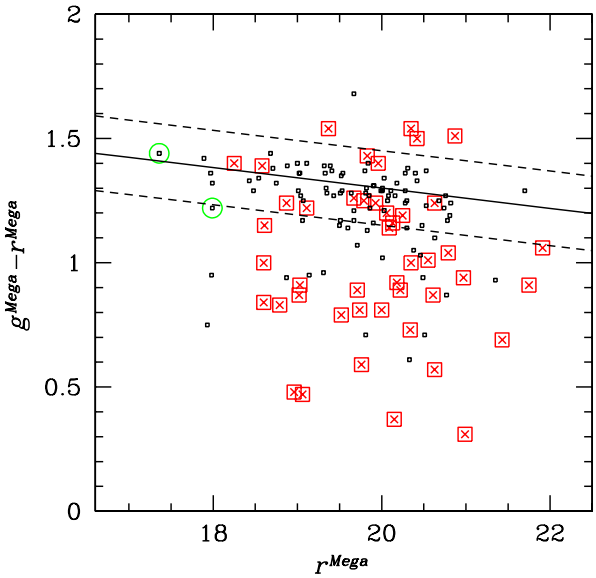

Fig. 7. CFHT $g^{\rm Mega}$–$r^{\rm Mega}$ vs. $r^{\rm Mega}$ diagram for galaxies with available spectroscopy. Small/black squares indicate member galaxies and large/red squares indicate nonmember galaxies. Red crosses indicate ELGs. The solid line gives the CMR determined on member galaxies; the dashed line is drawn at ±0.15 mag from this value. The green circles indicate the BCGN(NW) and BCGN(SE) of A1758N: these are the only galaxies of the sample that likely suffer for photon count saturation in the CFHT catalog (because they are brighter than $r^{\rm Mega} \sim 17$).

available in several magnitude bands, while the CFHT sample allows us to extend our analysis to fainter galaxies.

From the CFHT photometric catalog we selected likely cluster members on the basis of the ($g^{\rm Mega}$–$r^{\rm Mega}$) vs. $r^{\rm Mega}$ color-magnitude relation (hereafter CMR), which indicate the locus of the red-sequence galaxies. To determine the CMR we applied the 2σ-clipping fitting procedure to the spectroscopic cluster members. We obtained $g^{\rm Mega}$–$r^{\rm Mega} = 2.121$–$0.041 \times r^{\rm Mega}$ on 65 galaxies of our spectroscopic sample, which agrees very well with the CMR directly fitted on the photometric catalog recovered from CFHT images by Durret et al. (2011). Out of the CFHT photometric catalog, we considered as likely "red" cluster members the objects lying within 0.15 mag of the CMR, where ~0.15 is the error associated to the fitted intercept. Figure 7 shows that our selection criterion seems adequate to select red-sequence galaxies, which are good tracers of the cluster substructure (e.g., Lubin et al. 2000) and, above all, avoiding nonmember galaxies that might bias our 2D analysis. As for the sample with $r^{\rm Mega} \leq 21$, we can check our selection of likely members: we can recover 75% of spectroscopic members (i.e. 68 out of 90), but 30% of nonmembers are also selected (13 out of 42).

Figure 8 shows the galaxy density contours obtained with the 2D-DEDICA method for two samples: the CFHT likely members with $r^{\rm Mega} \leq 21$ and those with $21 < r^{\rm Mega} \leq 23$ (1657 and 3288 galaxies in the whole sample; 293 and 374 galaxies within 2 h_{70}^{-1} Mpc, respectively). As for the luminous galaxies, we found two very significant peaks along the SE-NW direction, corresponding to the BCGN(SE) and BCGN(NW): the NW-peak is the richest. These two peaks are separated by ~0.75 h_{70}^{-1} Mpc, with the SE-peak well coincident with the BCGN(SE) and the NW-peak at a distance of ~0.15 h_{70}^{-1} Mpc from the BCGN(NW). A third very significant peak lies in the South, coincident with the position of the cluster A1758S. As for the results with $r' \leq 21$, Table 2 lists the number of assigned members, $N_{\rm S}$ (Col. 2); the peak position (Col. 3); the density (in arbitrary units relative to the densest peak fixed to be 1), $\rho_{\rm S}$ (Col. 4); the value of χ^2 for each peak, $\chi^2_{\rm S}$ (Col. 5). The second sample (lower panel of Fig. 8) contains galaxies fainter by two mags: as discussed at the end of Sect. 4.1, these galaxies seem to trace the whole A1758N system and not its substructure.

Table 2. 2D substructure from the CFHT photometric sample.

Subclump	$N_{\rm S}{}^a$	α(J2000), δ(J2000) h:m:s, °:′:″	$\rho_{\rm S}$	$\chi^2_{\rm S}$
2D-N(NW) (CFHT $r^{\rm Mega} < 21$)	87	13 32 37.7+50 33 19	1.00	54
2D-S (CFHT $r^{\rm Mega} < 21$)	69	13 32 22.5+50 24 39	0.25	21
2D-N(SE) (CFHT $r^{\rm Mega} < 21$)	53	13 32 52.1+50 31 33	0.90	51

Notes. [(a)] Values are not background-subtracted.

When more than two colors are available, it is very effective to select cluster galaxies in the color–color space (Goto et al. 2002) and both SDSS r'–i' and g'–r' colors are generally used at $z < 0.4$ (Lu et al. 2009; Lopes 2007: his Eq. (1) and refs. therein). In particular, the difference between passive and star-forming galaxies is larger in g'–r' color than in r'–i' color (see Lu et al. 2009, their Fig. 6) but r'–i' color has a much smaller scatter (Lopes 2007, his Fig. 1). Out of the SDSS photometric catalog, we considered as likely "red" cluster members the objects lying within 0.1 and 0.2 mag of the CMRs (r'–i' vs. r') and (g'–r' vs. r'), respectively. When comparing this member selection to that performed on the CFHT catalog, we obtain a comparable result with a modest, better rejection of nonmembers. Indeed, we recover 67 out of 88 spectroscopic members and select only 10 out of 42 nonmembers (when using the g'–r' cut alone we obtain 67 out of 88 and 14 out of 42). As for the galaxy density map, the SDSS result confirms the result obtained with the bright CFHT sample: the NW-peak is still richer than the SE-peak (77 vs. 52 galaxies), although the SE-peak is now the densest (by a factor 1.5).

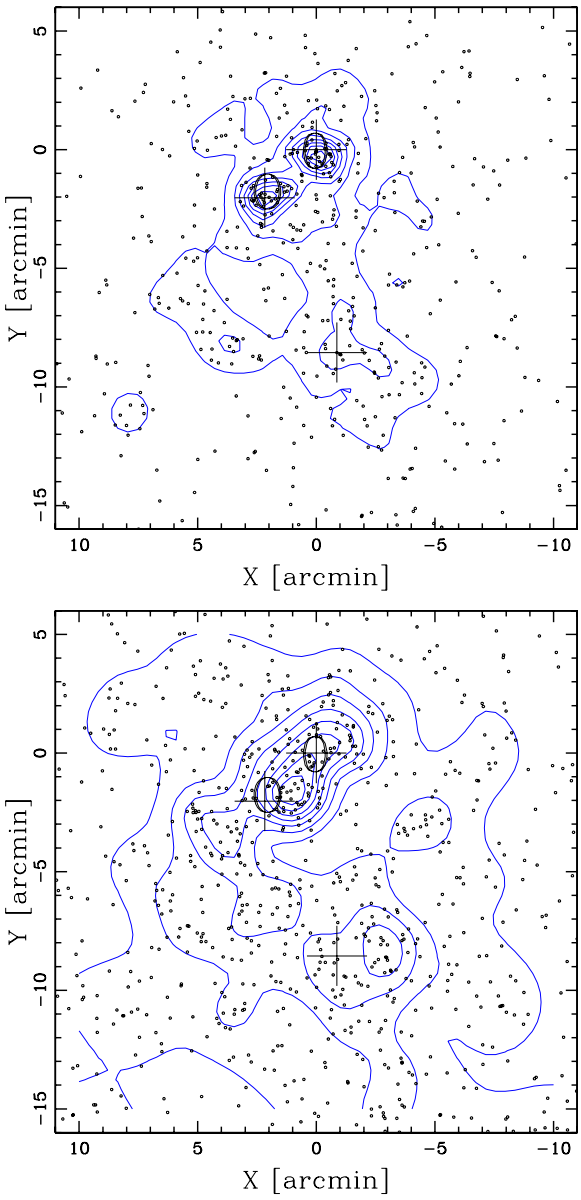

Fig. 8. Spatial distribution on the sky and relative isodensity contour map of CFHT photometric cluster members with $r^{\rm Mega} \leq 21$ (*upper panel*) and $21 < r^{\rm Mega} \leq 23$ (*lower panel*), obtained with the 2D-DEDICA method. The BCGN(NW) is taken as the cluster center. Northern crosses indicate the location of the BCGN(NW) and BCGN(SE) of A1758N. The southern cross indicates the BCGS of A1758S. For A1758N, the two large "O" labels are centered on the two main peaks of the mass distribution (Okabe et al. 2008).

3.5. 3D-analysis

The existence of correlations between positions and velocities of cluster galaxies is a characteristic of true substructures. Here we used several approaches to perform a 3D-analysis of the cluster.

We found no evidence for a significant velocity gradient (see, e.g., den Hartog & Katgert 1996; Girardi et al. 1996, for the details of the method).

We computed the Δ-statistics devised by Dressler & Schectman (1988, hereafter DS-test), which is recommended by Pinkney et al. (1996) as the most sensitive 3D test. For each galaxy, the deviation δ is defined as $\delta_i^2 = [(N_{\rm nn}+1)/\sigma_{\rm V}^2][(\overline{V}_{\rm l} - \overline{V})^2 + (\sigma_{\rm V,l} - \sigma_{\rm V})^2]$, where the subscript "l" denotes the local quantities computed over the $N_{\rm nn} = 10$ neighbors of the galaxy.

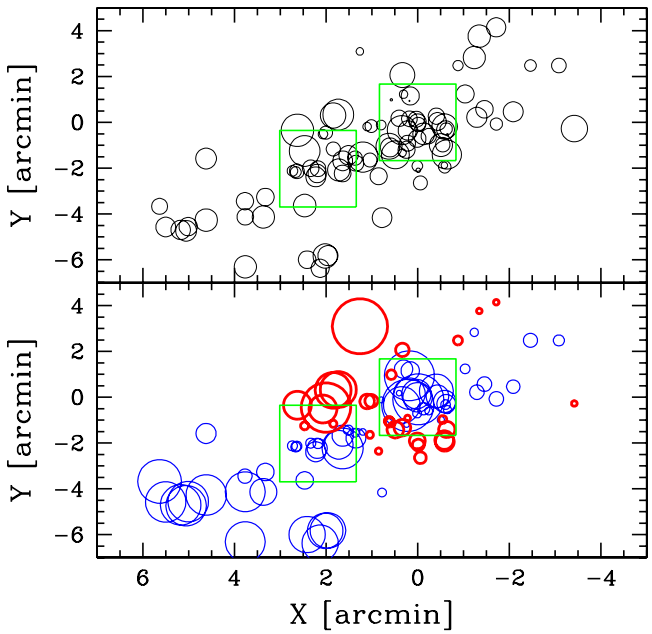

Fig. 9. Spatial distribution of the 92 cluster members, each marked by a circle. The BCGN(NW) is taken as the cluster center. *Upper panel*: the cluster velocity field: the larger the circle, the larger the galaxy velocity. *Lower panel*: the result of the (modified) DS-test: the larger the circle, the larger the deviation $\delta_{s,i}$ of the local velocity dispersion from the global velocity dispersion. Thin/blue and thick/red circles show where the local velocity dispersion is lower or higher than the global value. The two large green squares indicate the positions of the two BCGs.

Δ is the sum of the δ of the individual N galaxies and gives the cumulative deviation of the local kinematical parameters (mean velocity and velocity dispersion) from the global cluster parameters. The significance of Δ, i.e. of substructure, is checked by running 1000 Monte Carlo simulations, randomly shuffling the galaxy velocities. We found a significant presence of substructure at the 97% c.l.

Following Pinkney et al. (1996; see also Ferrari et al. 2003), we applied two more classical 3D tests: the ϵ-test (Bird 1993) based on the projected mass estimator and the centroid shift or α-test (West & Bothun 1990). The details of these tests can be found in the above papers. We merely point out that we considered ten as the number of the nearest neighbors for each galaxy and used Monte Carlo simulations to compute the substructure significance. The application of the ϵ-test leads to a significant presence of substructure at the 99.4% c.l.

To better understand the results of the DS-test described above, we also considered two kinematical estimators alternative to the δ parameter of the DS-test, i.e. we considered separately the contributes of the local mean $\delta_{\rm V}^2 = [(N_{\rm nn}+1)/\sigma_{\rm V}^2](\overline{V}_{\rm l} - \overline{V})^2]$, and dispersion $\delta_{\rm s}^2 = [(N_{\rm nn}+1)/\sigma_{\rm V}^2](\sigma_{\rm V,l} - \sigma_{\rm V})^2]$ (see, e.g. Girardi et al. 1997; Ferrari et al. 2003). When considering the $\delta_{\rm s}$ estimator, we found evidence for a peculiar local velocity dispersion at the 99.2% c.l. Figure 9 – lower panel – shows the distribution on the sky of all galaxies, each marked by a circle: the larger the circle, the larger the deviation $\delta_{{\rm s},i}$ of the local velocity dispersion from the global cluster value. Figure 9 shows: i) as A1758N(NW) is well detected as a region of low $\sigma_{\rm V,l}$, ii) a few galaxies in the NE central region have high values of $\sigma_{\rm V,l}$. The first result is expected for/interpreted as a system having a relaxed core owing to circular orbits or galaxy merger phenomena (i.e., Girardi et al. 1996, 1997; Menci & Fusco-Femiano 1996).

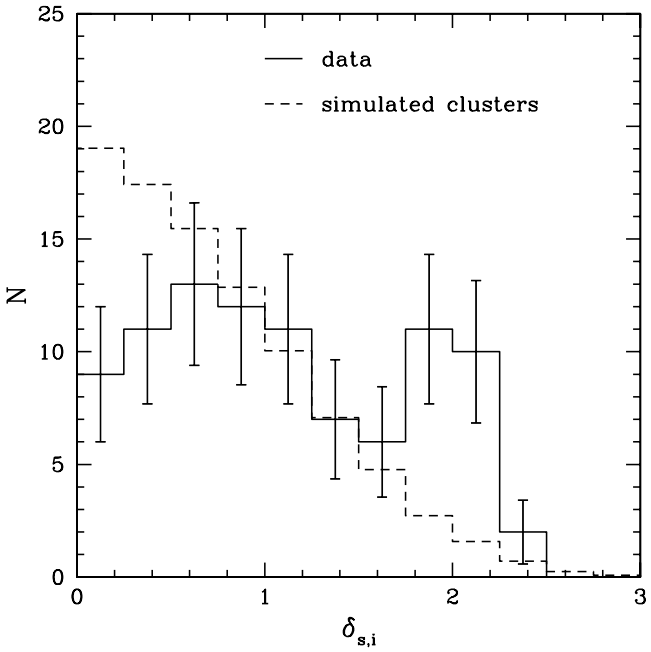

Fig. 10. Distribution of $\delta_{s,i}$ deviations of the Dressler-Schectman analysis for the 92 member galaxies. The solid line represents the observations with Poissonian errors. The dashed line is the distribution for the galaxies of simulated clusters, normalized to the observed number.

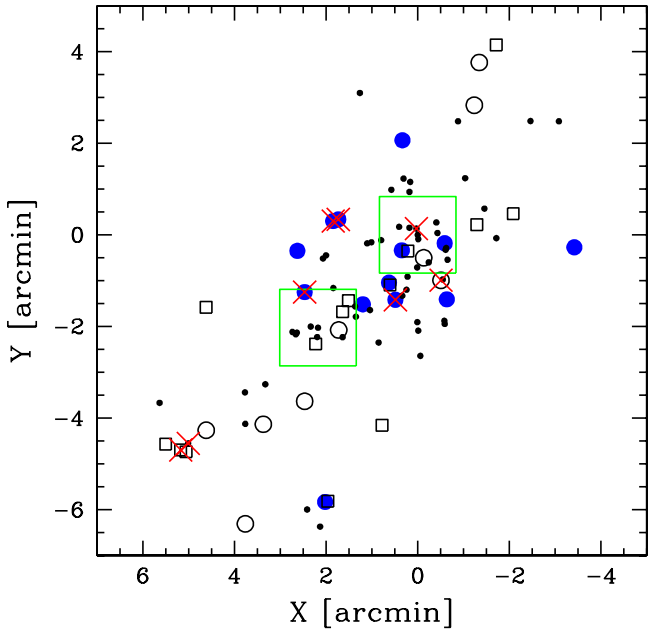

Fig. 11. Spatial distribution on the sky of the cluster galaxies, showing the four groups recovered by the weighted gap analysis. Solid/blue circles, open circles, open squares, and dots indicate the galaxies of GV1, GV2, GV3, and GV4, respectively. The BCGN(NW) is taken as the cluster center. Very large open green squares indicate the positions of BCGN(NW) and BCGN(SE). Large/red crosses indicate ELGs.

The second result deserves more attention: we compared the distribution of individual $\delta_{s,i}$ values of real galaxies with those of simulated clusters (Biviano et al. 2002). Figure 10 suggests that significantly high $\delta_{s,i}$ values for real data are those with $\delta_{s,i} > 1.8$. A part from several galaxies with peculiarly low $\sigma_{V,1}$, the 1.8 value only selects four galaxies with peculiarly high $\sigma_{V,1}$ (the largest thick/red circles in Fig. 9 – lower panel, IDs 81, 90, 93, and 96), two of which are ELGs.

Then we searched for a possible physical meaning of the four subclusters determined by the three weighted gaps. We compared the spatial galaxy distributions of GV1, GV2, GV3, and GV4 two by two. GV1 galaxies are distributed in a round region between the NW and the SE clumps, and do not follow the elongated shape of the sample. We verified that GV1 differs from GV3 (and from GV2+GV3) at the 94% c.l. (95% c.l.) according to the 2D Kolmogorov-Smirnov test (2DKS-test, Fasano et al. 1987, see Fig. 11).

We finally resorted to the method devised by Serna & Gerbal (1996, hereafter Htree-method; see, e.g., Durret et al. 2010, for a recent application). This method uses a hierarchical clustering analysis to determine the relationship between galaxies according to their relative binding energies. The method assumes a constant value for the mass-to-light ratio of galaxies and Serna & Gerbal (1996) suggested a value comparable to that of clusters. Here we took a value of $M/L_r = 150\ h_{70}\ M_\odot/L_\odot$, as suggested by large statistical studies (e.g., Girardi et al. 2000; Popesso et al. 2005).

Figure 12 shows the resulting dendogram, where the total energy appears horizontally. Galaxy pairs and subgroups of galaxies appear with a lower total energy. We note that there are no important subsystems. In particular, the BCGN(SE) and BCGN(NW) lie at the bottom of the potential well, although in two separate subsystems (a pair and a quadruplet, respectively). Instead, there are several small subsystems. We highlight here two that are situated at the highest energy levels, which might largely bias the computation of the global velocity dispersion.

In Fig. 12 we indicate HT2, a triplet of close galaxies at high velocity ($v > 87\,000$ km s^{-1}), and HT12, which is formed by seven galaxies ($v \sim 80\,000$ km s^{-1}) that lie in the central cluster region. Note that all seven galaxies of HT12 are also members of the GV1 group detected in our 1D analysis. Other significant subsystems of HT11, here interpreted as the main system, are small and generally formed by close galaxies. We suspect that their detection might be very sensitive to our incomplete spatial sampling and we do not discuss them. Figure 13 shows the spatial distributions of HT2 and HT12 with respect to the main system.

4. Discussion and conclusions

The high value of the velocity dispersion $\sigma_V = 1329^{+135}_{-116}$ km s^{-1} is comparable to the values found for hot, massive clusters (e.g., Mushotzky & Scharf 1997; Girardi & Mezzetti 2001). However, our estimate of σ_V is somewhat higher than the X-ray temperature of A1758N subclusters under the assumption of the equipartition of energy density between ICM and galaxies. Indeed, assuming that $kT_X \sim 7$ keV, we obtained $\beta_{spec} \sim 1.24$ to be compared with $\beta_{spec} = 1$, where $\beta_{spec} = \sigma_V^2/(kT_X/\mu m_p)$ with $\mu = 0.58$ the mean molecular weight and m_p the proton mass (see also Fig. 5). Indeed, our σ_V would instead predict a value of $kT_X = 10.7$ keV, which would be more in line with the temperature found in the region beyond the two cores, where the gas is already shocked by the merger and the X-ray temperature likely already enhanced to the value of the whole forming cluster (David & Kempner 2004, and discussion therein). Below we discuss the bimodal nature of A1758N.

4.1. Cluster structure and mass

In agreement with previous results (see Sect. 1), our 2D analysis highlights two subclusters in the galaxy distribution about

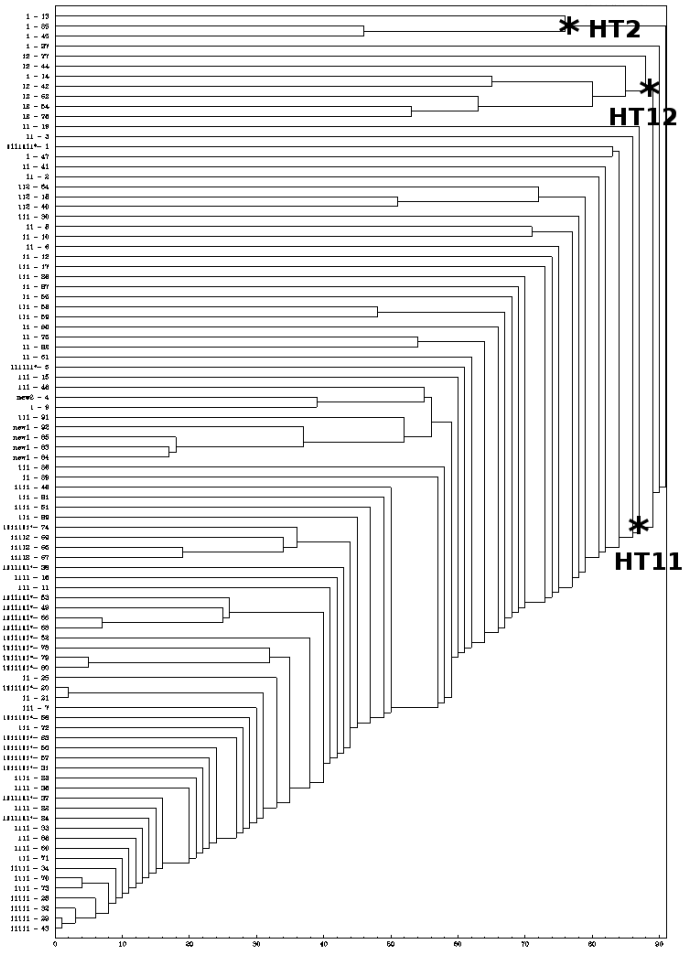

Fig. 12. Dendogram obtained through the Serna & Gerbal (1996) algorithm. The abscissa is the binding energy (here in arbitrary units with the deepest negative energy levels on the left) while the catalog numbers of the various member galaxies are shown along the ordinate (IDm in Table 1).

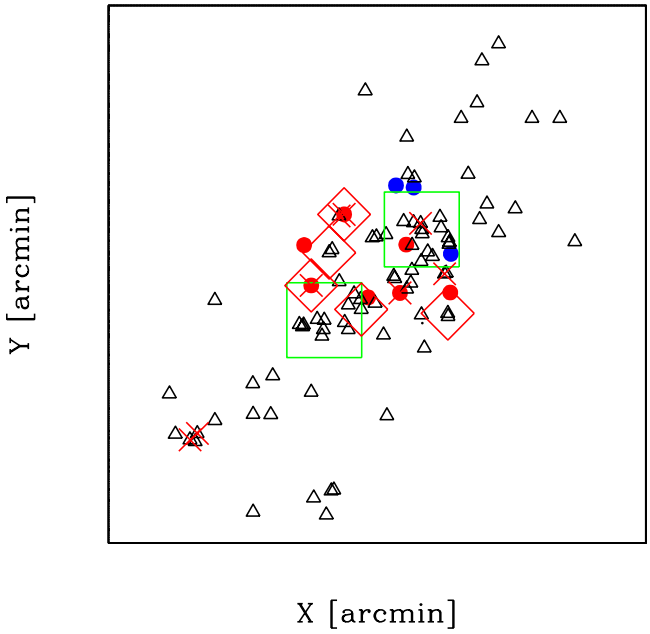

Fig. 13. Spatial distribution on the sky of the cluster galaxies showing the subsystems recovered by the Htree analysis. Solid blue and red circles indicate the galaxies of HT2 and HT12, respectively. Triangles indicate the galaxies of the main system (HT1). The BCGN(NW) is taken as the cluster center. Very large/green squares indicate the positions of BCGN(NW) and BCGN(SE). Large/red crosses indicate ELGs. Large red diamonds indicate dusty star-forming galaxies in the sample of Haines et al. (2009).

3′ (∼0.75 h_{70}^{-1} Mpc) away from each other along the SE-NW direction, hereafter A1758N(NW) and A1758N(SE).

We cannot separate A1758N(NW) and A1758N(SE) from the velocity information. Indeed, the small difference between the LOS velocities of the two BCGs ($\lesssim$300 km s^{-1} in the rest-frame) is by itself an indication that the two subclusters have low LOS relative velocity. In this study we were able to fully exploit our sample of 92 cluster members. From i) the inspection of the galaxy velocity field in Fig. 9 (upper panel), ii) the absence of a velocity gradient, iii) the absence of local velocity peculiarities via the DS-test, we confirm that the velocity difference between the two subclusters is very small. This is clearly shown by Fig. 14 – upper panel, where the integral mean velocities computed around A1758N(NW) and A1758N(SE) are very similar, lower than the velocity difference between the two BCGs.

Taking into account the similar velocities of the two BCGs, the sharp increase of the velocity dispersion profile within 0.5 h_{70}^{-1} Mpc (see Figs. 5 and 14 – faint red line – for both the subclusters) is not directly explainable with the presence of two systems at different mean velocity. Rather, this might be due to the presence of subclusters or individual galaxies infalling onto, or escaping from, the cluster. Indeed, beyond the usual infall onto the cluster from the large-scale structure, the recent merger of two subclumps may result in outflying galaxies as shown in simulations (e.g., Czoske et al. 2002) and seen in a few clusters (see e.g., the plume of outflying galaxies in Abell 3266 by Quintana et al. 1999; Flores et al. 2000; the structure of Cl0024+1654 by Czoske et al. 2002). In particular, the simulations reproducing Cl0024+1654 by Czoske et al. (2002) show that during a head-head collision at 3000 km s^{-1}, the outer regions of the smaller cluster have become unbound and are streaming radially away from the impact location with velocities perpendicular to the encounter on the order of 1000 km s^{-1}.

The velocity information is useful for detecting the galaxy groups connected with A1758N. Through our 3D Htree analysis we detected the high velocity HT2 group and the low velocity HT12 group. The HT2 and HT12 groups lie in the tails of the velocity distribution (which, in fact, is a heavy tailed distribution; see Sect. 3.3). In particular, HT12 is a subsample of GV1, the only group detected in the 1D analysis that also has a peculiar spatial distribution. Spatially, HT2 and HT11 lie in the central region roughly between the two BCGs, where, in the NE, the DS analysis detects a region of high local velocity dispersion. Figure 14 – lower panel – shows the resulting profile of the velocity dispersion when only the main system HT11 is considered: the effect is that the value of σ_V decreases to ∼1000 km s^{-1}.

As for individual/peculiar galaxies, we highlight the NAT galaxy 1330+507 (ID 105). Head-tail and NAT radio galaxies are most common in clusters with perturbed X-ray morphologies and are probably produced while radio galaxies move through cluster atmospheres at high velocities (Burns et al. 1994). Here the NAT galaxy was rejected in the second step of our member selection procedure (the galaxy represented by the square with the lowest velocity at $R \sim 0.7\ h_{70}^{-1}$ Mpc in Fig. 5 – top panel) and therefore it is likely to be a galaxy "at the border" of the phase-space distribution of A1758N. The NAT, projected onto close BCGN(SE), points toward A1758N(NW) (see Fig. 1), which suggests that it is infalling onto the cluster center.

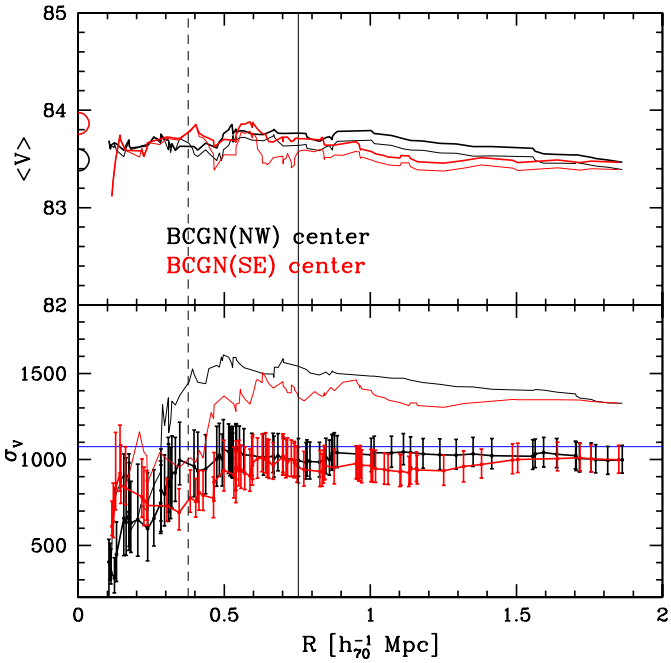

Fig. 14. *Upper and lower panels:* integral profiles of mean velocity and LOS velocity dispersion, respectively. Black and red lines consider as centers BCGN(NW) and BCG(SE), respectively. In both panels the vertical solid lines indicate the distance of the BCG of the close subcluster and the dashed lines indicate the half distance. Thin and thick lines give the results for all galaxies and the main system HT11. In the upper panel, the two semi-circles give the velocity of the two BCGs. In the lower panel, the horizontal line represents the X-ray temperature as in Fig. 5.

In their analysis of galaxies with *Spitzer*/MIPS 24 μm emission in the region of A1758, Haines et al. (2009) stressed that these dusty star-forming galaxies trace the cluster potential and in particular the core of A1758N. This supports the hypothesis that activity in clusters is triggered by the cluster-cluster merger (i.e. is due to the passage of gas-rich galaxies through shocked regions of the ICM or affected by time-dependent cluster tidal fields, e.g., Roettiger et al. 1996; Bekki 1999; Bekki et al. 2010). However, they used photometric redshifts to establish the A1758 membership, while we were able to use spectroscopic redshifts to asses their result. We have redshifts for twelve galaxies out of infrared luminous galaxies plotted in their Fig. 1 (blue circles). Out of these twelve galaxies, five are cluster members and they indeed lie in the core of A1758N, between the two BCGs, thus supporting the conclusions of Haines et al. (2009; see large red diamonds in Fig. 13). Moreover, another four luminous infrared galaxies were rejected from the cluster members only at the second step of our procedure, i.e. they lie "at the border" of the projected phase-space distribution shown in Fig. 5 (top panel). Very interestingly, galaxies with emission lines have a similar behavior: all 14 ELGs in our spectroscopic catalog are connected to the cluster, eight of them belonging to the cluster and six at the border (see Fig. 5). In particular, six out of the eight members are embedded in the cluster core (see Fig. 13). Thus, also the ELGs support the hypothesis that activity in A1758N is triggered by the cluster-cluster merger. The effect of the cluster merger on the galaxy population was also suggested by Durret et al. (2011), who found an excess of very bright galaxies and a bump at $M_{r'} \sim -17$ in the observed luminosity function with respect to a Schechter luminosity function.

Here we discuss the relative importance of the NW and SE subclusters. From the galaxy clump luminosities, Okabe & Umetsu (2008) suggested that A1758N(NW) is the primary component and A1758N(SE) is the merging substructure, but they measured similar velocity dispersions ($\sigma_{V,SIS} \sim$ 600–700 km s^{-1}) from their weak-lensing analysis. This conclusion also agrees with the fact that A1758N(SE) shows an offset with the respective X-ray peak and A1758N(NW) does not. Our 2D-DEDICA analysis shows that A1758N(NW) is richer than A1758N(SE), which suggests that A1758N(NW) is the main structure. On the other hand, the SE peak shows a comparable density (see Table 2). This supports the idea that A1758N(SE) is the surviving, dense core of a merging structure. The determination of the velocity dispersion of subclusters is often a difficult task. Figure 14 – lower panel – shows the σ_V profiles using alternatively BCGN(NW) or BCGN(SE) as centers. As for A1758N(NW), the value of its σ_V is progressively increasing – which agrees with the small core with peculiar low local σ_V shown by the DS-test – out to ~1000 km s^{-1}. As for A1758N(SE), the value of its σ_V is mostly stable at ~700–800 km s^{-1} before increasing at about half the distance from A1758N(NW). Considering the large errors, there is no significant difference between the values of σ_V of A1758N(NW) and A1758N(SE). However, in agreement with the idea that A1758N(NW) is the main system, below we consider the nominal values at the half distance, i.e. $\sigma_{V,NW} \sim 1000$ km s^{-1} and $\sigma_{V,SE} \sim 800$ km s^{-1} for A1758N(NW) and A1758N(SE), respectively.

Making the usual assumptions for the two subclusters (cluster sphericity, dynamical equilibrium, coincidence of the galaxy and mass distributions), we can compute virial global quantities. We followed the prescriptions of Girardi & Mezzetti (2001; see also Girardi et al. 1998) and computed R_{vir} – an estimate for R_{200} – and the mass contained within this radius. In particular, we assume for the radius of the quasi-virialized region $R_{vir} = 0.17 \times \sigma_V / H(z)\ h_{70}^{-1}$ Mpc (see Eq. (1) of Girardi & Mezzetti 2001; with the scaling of $H(z)$ of Eq. (8) of Carlberg et al. 1997, for R_{200}). For the mass we used the virial mass corrected for the surface pressure term correction $M = M_V - SPT = 3\pi/2 \cdot \sigma_V^2 R_{PV}/G - SPT$ (Eq. (3) of Girardi & Mezzetti 2001), with the size estimate R_{PV} computed using the full procedure based on an assumed typical galaxy distribution and $SPT = 0.2 \times M_V$. In practice, both R_{vir} and M were computed on the basis of the estimated velocity dispersion with the usual scaling-laws, where $R_{vir} \propto \sigma_V$ and $M(<R_{vir}) \propto \sigma_V^3$. We computed $M_{NW}(<R_{vir} = 2.1\ h_{70}^{-1}$ Mpc$) = 1.4 \times 10^{15}\ h_{70}^{-1}\ M_\odot$ and $M_{SE}(<R_{vir} = 1.7\ h_{70}^{-1}$ Mpc$) = 0.7 \times 10^{15}\ h_{70}^{-1}\ M_\odot$ for the NW and SE subsystems, respectively. We computed a mass $M_{sys}(<R = 2.1\ h_{70}^{-1}$ Mpc$) \gtrsim 2.1 \times 10^{15}\ h_{70}^{-1}\ M_\odot$ for the whole system, depending on how far we extrapolated the mass of A1758N(SE) outside its R_{vir}. This value agrees with the value we obtained assuming the whole system to be relaxed $M(<R_{vir} = 2.8\ h_{70}^{-1}$ Mpc$) = 3 \pm 1 \times 10^{15}\ h_{70}^{-1}\ M_\odot$ when rescaled to the smaller $R = 2.1\ h_{70}^{-1}$ Mpc radius.

As for the cluster structure, finally we discuss our result of faint galaxies tracing a peak intermediate between the two BCGs, somewhat close to the secondary X-ray peak, while luminous galaxies trace two subclusters (see Fig. 8). This phenomenon of luminosity segregation can be connected with the cluster internal dynamics. Indeed, very appealingly, galaxies of different luminosity could trace the dynamics of cluster mergers in a different way. A first evidence was provided by Biviano et al. (1996): they found that the two central dominant galaxies

of the Coma cluster are surrounded by luminous galaxies, accompanied by the two main X-ray peaks, while the distribution of faint galaxies tends to form a structure not centered with one of the two dominant galaxies, but is instead coincident with a secondary peak detected in X-ray data. The observational scenario of Abell 209 has some peculiar luminosity segregation, too (Mercurio et al. 2003). Therefore, following Biviano et al. (1996), we speculate that the merging is in a post-merging phase, where faint galaxies trace the forming structure of the cluster in formation, while more luminous galaxies still trace the remnant of the core-halo structure of pre-merging subclusters.

4.2. Merger kynematics and diffuse radio sources

Although member galaxies can give some pieces of evidence in favor of a post-merger phase, the stringent proof is given by the X-ray analysis of David & Kempner (2004, *Chandra* and *XMM-Newton* data) who detected shock-heated gas around the cores of the two subclusters. In this study we obtained some important properties of the merger: the LOS relative velocity is $\lesssim$300 km s^{-1} and the merger is a major merger with a mass ratio of ~(2:1). Moreover, in agreement with the results of Pinkney et al. (1996), the fact that we clearly detected the subclusters in 2D, but not in the 1D and 3D analyses, suggests that the plane of the cluster merger is mostly perpendicular to the LOS. This would also explain the good observability of the X-ray morphological features.

Figure 1 shows the comparison between the positions of the density peaks in the galaxy distribution obtained in this work and the results from other wavelengths. In agreement with the fact that elongated radio halos normally follow the merging direction (e.g., the "bullet" cluster by Markevitch et al. 2002; Abell 520 by Girardi et al. 2008; Abell 754 by Macario et al. 2011), the halo of A1758N is clearly elongated along the NW-SE direction. As for the two relics, the eastern one (R1 in Fig. 1) is not perpendicular to the merging axis, as it is typically found in double relic clusters (e.g., Abell 3667 Roettiger et al. 1999; Kempner & Sarazin 2001). This supports the idea that A1758N is not a head-on merger (see below, but see Bonafede et al. 2009; and Boschin et al. 2010, for alternative explanations of non-symmetric radio relics in Abell 2345). More quantitatively, we can use our results to examine A1758N with respect to the observed scaling relation between $P_{1.4\,\mathrm{GHz}}$, the halo radio power, and the total cluster mass (as determined within 3 h_{70}^{-1} Mpc, Govoni et al. 2001). Considering the value of $P_{1.4\ \mathrm{GHz}} = 9.3 \times 10^{23}$ W Hz^{-1} by Giovannini et al. (2009) and our $M_{\mathrm{sys}} = 2$–$3 \times 10^{15}\ h_{70}^{-1}\ M_{\odot}$, A1758N results to be an under-radio-luminous cluster (see Fig. 18 of Govoni et al. 2001). However, it should be said that A1758N is also very peculiar because of the presence of the two close relics. When considering the total diffuse emission radio+relics $P_{1.4\ \mathrm{GHz}} = 4 \times 10^{24}$ W Hz^{-1} (Giovannini et al. 2009), there is no longer a discrepancy.

The presence of the diffuse radio emissions suggests that A1758N probably is a recent merger because they are expected to have a short life time, i.e. on the order of a few fractions of Gyr (e.g., Giovannini & Feretti 2002; Skillman et al. 2011). For radio halos, present estimates of the time elapsed after the core-core crossing are very short (e.g., 0.1–0.2 Gyr in the "bullet" cluster by Markevitch et al. 2002; 0.2–0.3 in Abell 520 by Girardi et al. 2008). Times are somewhat longer for the radio relics (1 Gyr in Abell 3667 by Roettiger et al. 1999), but they refer to clusters whose relics are separated by $\gtrsim 2\ h_{70}^{-1}$ Mpc, therefore we expect that the times for A1758N relics are shorter. An independent

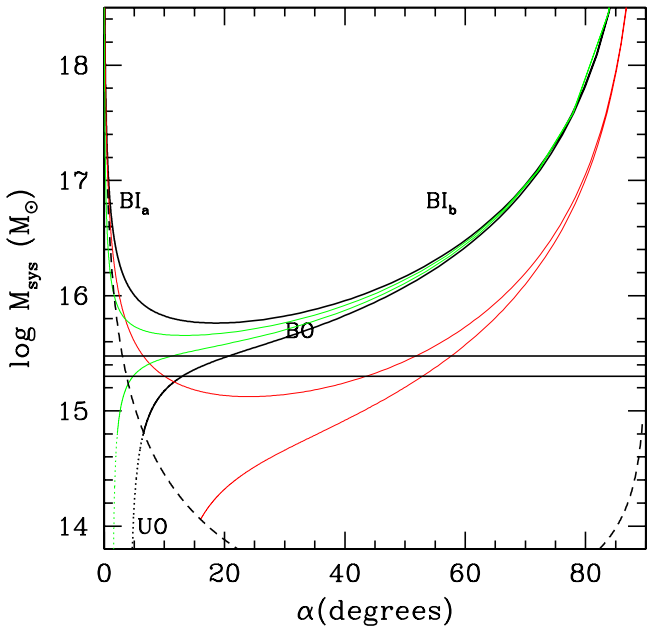

Fig. 15. System mass vs. projection angle for bound and unbound solutions (thick solid and thick dashed curves, respectively) of the two-body model applied to the A1758N(NW) A1758N(SE) subclusters. Thick/black lines refer to $t = 0.2$ Gyr and $V_{\mathrm{rf,LOS}} = 300$ km s^{-1}. Labels $\mathrm{BI_a}$ and $\mathrm{BI_b}$ indicate the bound and incoming, i.e., collapsing solutions (solid curve). Labels BO and UO indicate the bound outgoing, i.e., expanding solutions and unbound outgoing solutions (solid curve going on in the dotted curve, respectively). The horizontal lines give the range of observational values of the mass system. The dashed curve separates bound and unbound regions according to the Newtonian criterion (above and below the thin dashed curve, respectively). The red/faint lines refer to $t = 0.5$ Gyr and $V_{\mathrm{rf,LOS}} = 300$ km s^{-1}. The green/faint lines refer to $t = 0.2$ Gyr and $V_{\mathrm{rf,LOS}} = 100$ km s^{-1}.

evidence of the early age of the cluster merger comes from the presence of the bump of highly star-forming galaxies in the cluster core, being the duration of the strong starburst induced by the cluster merger of <0.5 Gyr (Bekki 1999).

On the basis of our results we investigated the relative dynamics of A1758N and A1758S using different analytic approaches, that are based on an energy integral formalism in the framework of locally flat spacetime and Newtonian gravity (e.g., Beers et al. 1982). The values of the relevant observable quantities for the two-clumps system are the relative LOS velocity in the rest frame, $V_{\mathrm{r}} = 300$ km s^{-1} (which is an upper limit); the projected linear distance between the two clumps, $D \sim 0.8\ h_{70}^{-1}$ Mpc; the mass of the system $M_{\mathrm{sys}} = 2$–$3 \times 10^{15}\ h_{70}^{-1}\ M_{\odot}$. First, we considered the Newtonian criterion for gravitational binding stated in terms of the observables as $V_{\mathrm{r}}^2 D \leq 2GM_{\mathrm{sys}} \sin^2\alpha \cos\alpha$, where α is the projection angle between the plane of the sky and the line connecting the centers of two clumps. The dashed curve in Fig. 15 separates the bound and unbound regions according to the Newtonian criterion (above and below the curve, respectively). The system is bound between ~3° and 90°; the corresponding probability, computed considering the solid angles (i.e., $\int_5^{90} \cos\alpha\, \mathrm{d}\alpha$), is 95%. We also considered the implemented criterion $V_{\mathrm{r}}^2 D \leq 2GM \sin^2\alpha_{\mathrm{V}} \cos\alpha_{\mathrm{D}}$, which introduces different angles for projection of distance and velocity, not assuming a strictly radial motion between the clumps (Hughes et al. 1995). We obtained a binding probability of 94%.

In the simple case of a strictly radial motion we can check if the merger kinematics agrees with the idea of a very recent merger because the simple linear-orbit two-body model connects the time elapsed from the the core-core passage t and the projection angle α. Figure 15 shows the bimodal-model solutions as a function of α. The thick/black lines show the case with $V_{\rm rf,LOS} = 300$ km s^{-1}and the time from the core-core passage $t = 0.2$ Gyr. There is a bound outgoing solution (BO) with $\alpha \sim 15$–$20°$ that leads to a deprojected relative velocity of $V_{\rm rf} \sim 1150$–900 km s^{-1}. The effect of decreasing the relative velocity is that of decreasing the projection angle, e.g. $V_{\rm rf,LOS} = 100$ km s^{-1} leads to $\alpha \sim 5$–$10°$ and thus to $V_{\rm rf} \gtrsim 1150$–600 km s^{-1}. The effect of increasing the age of the merger is that of increasing the projection angle and decreasing the relative velocity, e.g. $t = 0.5$ Gyr leads to $\alpha \sim 55$–$60°$ and thus to $V_{\rm rf} \sim 350$ km s^{-1} (here there are also two symmetric bound incoming solutions). Therefore only a very recent merger agrees with the evidence that the merger plane is mostly perpendicular to the LOS. Moreover, we have to consider the limits on the relative velocity indirectly recovered from X-ray data. In order to produce the shock waves, which e.g. originate the relics, we need a Mach number $\mathcal{M} > 1$ and David & Kempner (2004) computed $\mathcal{M} \lesssim 1.15$ from X-ray data. The Mach number is defined to be $\mathcal{M} = v_{\rm s}/c_{\rm s}$, where $v_{\rm s}$ is the velocity of the shock and $c_{\rm s}$ in the sound speed in the pre-shock gas (see e.g., Sarazin 2002, for a review). Assuming for the sound speed in the pre-shock gas the value obtained from the X-ray temperature of David & Kempner (6–9 keV), i.e. $v_{\rm s} = 1000$–1200 km s^{-1}, and $v_{\rm s} \sim V_{\rm rf}$, we expect $V_{\rm rf}$ to be in the range of 1000–1300 km s^{-1}, which agrees with models with a very recent merger.

The obvious limit of the model described above is that the merger is treated as a head-on merger. Although general arguments suggest small impact parameters for cluster mergers ($\sim 0.2\ h_{70}^{-1}$ Mpc, see Sarazin 2002), it seems that this is not the case for A1758N. From the morphological details of the X-ray surface brightness image, David & Kempner (2004) deduced that the NW subcluster is moving north and the SE subcluster is moving southeast and that A1758N is in the late stage of a large impact parameter merger: their Fig. 9 shows the proposed orbits in the merging plane. However, these orbits are not supported by the two elongated regions of high metallicity likely left by ram-pressure stripping during the merger (Sect. 4 and Fig. 13 of Durret et al. 2011): the NW feature is elongated along NW-SE as in the case of a head-on merger, while the SW feature has a clear tail perpendicular to the NW-SE direction as in the case of an off-axis merger. Thus, to date, we are far from knowing the details of the possible orbits and from investigating a more complex kinematics.

Our general conclusions about A1758 agree with other typical clusters that show extended diffuse radio emissions, i.e. we are dealing with a massive cluster with a major ongoing merger (like, e.g., Abell 2744; see Boschin et al. 2006) and, indeed, less massive merging systems do not seem to host extended radio emissions (e.g. Abell 2146 by Russell et al. 2011; see also Rodríguez-Gonzálvez et al. 2011).

Acknowledgements. W.B. dedicates this study to the memory of his father, Andriano Boschin, deceased on November 15, 2011. We acknowledge Federica Govoni and Gabriele Giovannini for the VLA radio image they kindly provided us and their useful comments. We also thank the anonymous referee for his/her stimulating comments and suggestions. This publication is based on observations made on the island of La Palma with the Italian Telescopio Nazionale Galileo (TNG). The TNG is operated by the Fundación Galileo Galilei – INAF (Istituto Nazionale di Astrofisica) and is located in the Spanish Observatorio of the Roque de Los Muchachos of the Instituto de Astrofisica de Canarias. This research has made use of the NASA/IPAC Extragalactic Database (NED), which is operated by the Jet Propulsion Laboratory, California Institute of Technology, under contract with the National Aeronautics and Space Administration. This research has made use of archival data obtained at the Canada-France-Hawaii Telescope (CFHT), which is operated by the National Research Council of Canada, the Institut National des Sciences de l'Univers of the Centre National de la Recherche Scientifique of France, and the University of Hawaii. This research has made use of the galaxy catalog of the Sloan Digital Sky Survey (SDSS). Funding for the SDSS has been provided by the Alfred P. Sloan Foundation, the Participating Institutions, the National Aeronautics and Space Administration, the National Science Foundation, the US Department of Energy, the Japanese Monbukagakusho, and the Max Planck Society. The SDSS Web site is http://www.sdss.org/. The SDSS is managed by the Astrophysical Research Consortium for the Participating Institutions. The Participating Institutions are the American Museum of Natural History, Astrophysical Institute Potsdam, University of Basel, University of Cambridge, Case Western Reserve University, University of Chicago, Drexel University, Fermilab, the Institute for Advanced Study, the Japan Participation Group, Johns Hopkins University, the Joint Institute for Nuclear Astrophysics, the Kavli Institute for Particle Astrophysics and Cosmology, the Korean Scientist Group, the Chinese Academy of Sciences (LAMOST), Los Alamos National Laboratory, the Max-Planck-Institute for Astronomy (MPIA), the Max-Planck-Institute for Astrophysics (MPA), New Mexico State University, Ohio State University, University of Pittsburgh, University of Portsmouth, Princeton University, the United States Naval Observatory, and the University of Washington.

References

Abell, G. O., Corwin, H. G. Jr., & Olowin, R. P. 1989, ApJS, 70, 1
Ashman, K. M., Bird, C. M., & Zepf, S. E. 1994, AJ, 108, 2348
Bardelli, S., Zucca, E., Vettolani, G., et al. 1994, MNRAS, 267, 665
Barrena, R., Girardi, M., Boschin, W., & Dasí, M. 2009, A&A, 503, 357
Beers, T. C., Geller, M. J., & Huchra, J. P. 1982, ApJ, 257, 23
Beers, T. C., Flynn, K., & Gebhardt, K. 1990, AJ, 100, 32
Beers, T. C., Forman, W., Huchra, J. P., Jones, C., & Gebhardt, K. 1991, AJ, 102, 1581
Beers, T. C., Gebhardt, K., Huchra, J. P., et al. 1992, ApJ, 400, 410
Bekki, K. 1999, ApJ, 510, L15
Bekki, K., Owers, M. S., & Couch, W. J. 2010, ApJ, 718, L27
Bird, C. M., & Beers, T. C. 1993, AJ, 105, 1596
Biviano, A., Durret, F., Gerbal, D., et al. 1996, A&A, 311, 95
Biviano, A., Katgert, P., Thomas, T., & Adami, C. 2002, A&A, 387, 8
Bonafede, A., Feretti, L., Giovannini, G., et al. 2009, A&A, 503, 707
Boschin, W., Girardi, M., Spolaor, M., & Barrena, R. 2006, A&A, 449, 461
Boschin, W., Barrena, R., & Girardi, M. 2010, A&A, 521, A78
Brunetti, G., Cassano, R., Dolag, K., & Setti, G. 2009, A&A, 507, 661
Buote, D. A. 2002, in Merging Processes in Galaxy Clusters, ed. L. Feretti, I. M. Gioia, & G. Giovannini (The Netherlands: Kluwer Ac. Pub.), 79
Burns, J. O., Roettiger, K., Ledlow, M., & Klypin, A. 1994, ApJ, 427, L87
Carlberg, R. G., Yee, H. K. C., & Ellingson, E. 1997, ApJ, 478, 462
Cassano, R., & Brunetti, G. 2005, MNRAS, 357, 1313
Cassano, R., Brunetti, G., & Setti, G. 2006, MNRAS, 369, 1577
Cassano, R., Brunetti, G., Röttgering, H. J. A., & Brüggen, M. 2010a, A&A, 509, A68
Cassano, R., Ettori, S., Giacintucci, S., et al. 2010b, ApJ, 721, L82
Czoske, O., Moore, B., Kneib, J.-P., & Soucail, G. 2002, A&A, 386, 31
Dahle, H., Kaiser, N., Irgens, R. J., Lilje, P. B., & Maddox, S. J. 2002, ApJS, 139, 313
Danese, L., De Zotti, C., & di Tullio, G. 1980, A&A, 82, 322
David, L. P., & Kempner, J. 2004, ApJ, 613, 831
den Hartog, R., & Katgert, P. 1996, MNRAS, 279, 349
Dressler, A., & Shectman, S. A. 1988, AJ, 95, 985
Durret, F., Laganá, T. F., Adami, C., & Bertin, E. 2010, A&A, 517, A94
Durret, F., Laganá, T. F., & Haider, M. 2011, A&A, 529, A38
Ebeling, H., Edge, A. C., Böhringer, H., et al. 1998, MNRAS, 301, 881
Ellingson, E., & Yee, H. K. C. 1994, ApJS, 92, 33
Ensslin, T. A., & Gopal-Krishna 2001, A&A, 366, 26
Ensslin, T. A., Biermann, P. L., Klein, U., & Kohle, S. 1998, A&A, 332, 395
Ensslin, T. A., Pfrommer, C., Miniati, F., & Subramanian, K. 2011, A&A, 527, A99
Fadda, D., Girardi, M., Giuricin, G., Mardirossian, F., & Mezzetti, M. 1996, ApJ, 473, 670
Fasano, G., & Franceschini, A. 1987, MNRAS, 225, 155
Feretti, L. 1999, MPE Report No. 271
Feretti, L. 2002a, The Universe at Low Radio Frequencies, Proc. IAU Symp., 199, held 30 Nov.–4 Dec. 1999, Pune, India, ed. A. Pramesh Rao, G. Swarup, & Gopal-Krishna, 133
Feretti, L. 2005, X-Ray and Radio Connections, ed. L. O. Sjouwerman, & K. K. Dyer, Published electronically by NRAO, http://www.aoc.nrao.edu/

events/xraydio, held 3–6 February 2004 in Santa Fe, New Mexico, USA
Feretti, L., Gioia I. M., & Giovannini, G. 2002b, Merging Processes in Galaxy Clusters (The Netherlands: Kluwer Academic Publisher), Astrophys. Space Sci. Lib., 272
Feretti, L., Schuecker, P., Böhringer, H., Govoni, F., & Giovannini, G. 2005, A&A, 444, 157
Ferrari, C., Maurogordato, S., Cappi, A., & Benoist, C. 2003, A&A, 399, 813
Flores, R. A., Quintana, H., & Way, M. J. 2000, ApJ, 532, 206
Giovannini, G., & Feretti, L. 2002, in Merging Processes in Galaxy Clusters, ed. L. Feretti, I. M. Gioia, & G. Giovannini (The Netherlands: Kluwer Ac. Pub.), Diffuse Radio Sources and Cluster Mergers
Giovannini, G., Tordi, M., & Feretti, L. 1999, New Astron., 4, 141
Giovannini, G., Feretti, L., Govoni, F., et al. 2006, Astron. Nachr., 327, 563
Giovannini, G., Bonafede, A., Feretti, L., et al. 2009, A&A, 507, 1257
Girardi, M., & Biviano, A. 2002, in Merging Processes in Galaxy Clusters, ed. L. Feretti, I. M. Gioia, & G. Giovannini (The Netherlands: Kluwer Ac. Pub.), 39
Girardi, M., & Mezzetti, M. 2001, ApJ, 548, 79
Girardi, M., Fadda, D., Giuricin, G. et al. 1996, ApJ, 457, 61
Girardi, M., Escalera, E., Fadda, D., et al. 1997, ApJ, 482, 11
Girardi, M., Giuricin, G., Mardirossian, F., Mezzetti, M., & Boschin, W. 1998, ApJ, 505, 74
Girardi, M., Borgani, S., Giuricin, G., Mardirossian, F., & Mezzetti, M. 2000, ApJ, 530, 62
Girardi, M., Barrena, R., & Boschin, W. 2007, Contribution to Tracing Cosmic Evolution with Clusters of Galaxies: Six Years Later, conference – http://adlibitum.oat.ts.astro.it/girardi/darc/sestomgirardi.pdf
Girardi, M., Barrena, R., Boschin, W., & Ellingson, E. 2008, A&A, 491, 379
Goto, T., Sekiguchi, M., Nichol, R. C., et al. 2002, AJ, 123, 1807
Govoni, F., Feretti, L., Giovannini, G., et al. 2001, A&A, 376, 803
Gwyn, S. D. 2009, in Astronomical Data Analysis Software and Systems XVIII, ASP Conf. Ser., 411, 123
Haines, C. P., Smith, G. P., Egami, E., et al. 2009, MNRAS, 396, 1297
Hart, Q. N., Stocke, J. T., & Hallman, E. J. 2009, ApJ, 705, 854
Hoeft, M., Brüggen, M., & Yepes, G. 2004, MNRAS, 347, 389
Hughes, J. P., Birkinshaw, M., & Huchra, J. P. 1995, ApJ, 448, 93
Kempner, J. C., & Sarazin, C. L. 2001, ApJ, 548, 639
Kempner, J. C., Blanton, E. L., Clarke, T. E., et al. 2004, Proc. Conf., The Riddle of Cooling Flows in Galaxies and Clusters of Galaxies, ed. T. H. Reiprich, J. C. Kempner, & N. Soker [arXiv:astro-ph/0310263]
Kennicutt, R. C. 1992, ApJS, 79, 225
Keshet, U., & Loeb, A. 2010, ApJ, 722, 737
Lopes, P. A. A. 2007, MNRAS, 380, 1608
Lu, T., Gilbank, D. G., Balogh, M. L., & Bognat, A. 2009, MNRAS, 399, 1858
Lubin, L. M., Brunner, R., Metzger, M. R., Postman, M., & Oke, J. B. 2000, ApJ, 531, 5
Malumuth, E. M., Kriss, G. A., Dixon, W. V. D., Ferguson, H. C., & Ritchie, C. 1992, AJ, 104, 495
Markevitch, M., Gonzalez, A. H., David, L., et al. 2002, ApJ, 567, L27
Macario, G., Markevitch, M., Giacintucci, S., et al. 2011, ApJ, 728, 82
Mercurio, A., Girardi, M., Boschin, W., Merluzzi, P., & Busarello, G. 2003, A&A, 397, 431
Menci, N., & Fusco-Femiano, R. 1996, ApJ, 472, 46
Mushotzky, R. F., & Scharf, C. A. 1997, ApJ, 482, L13
O'Dea, C. P., & Owen, F. N. 1985, AJ, 90, 927
Okabe, N., & Umetsu, K. 2008, PASJ, 60, 345
Pinkney, J., Roettiger, K., Burns, J. O., & Bird, C. M. 1996, ApJS, 104, 1
Pisani, A. 1993, MNRAS, 265, 706
Pisani, A. 1996, MNRAS, 278, 697
Popesso, P., Biviano, A., Böhringer, H., Romaniello, M., & Voges, W. 2005, A&A, 433, 431
Quintana, H., Ramírez, A., & Way, M. J. 1996, AJ, 112, 360
Quintana, H., Carrasco, E. R., & Reisenegger, A. 2000, AJ, 120, 511
Ragozzine, B., Clowe, D., Markevitch, M., Gonzalez, A. H., & Bradač, M. 2012, ApJ, 744, 94
Rizza, E., Burns, J. O., Ledlow, M. J., et al. 1998, MNRAS, 301, 328
Rizza, E., Morrison, G. E., Owen, F. N., et al. 2003, AJ, 126, 119
Rodríguez-Gonzálvez, C., Olamaie, M., Davies, M. L., et al. 2011, MNRAS, 414, 3751
Roettiger, K., Burns, J. O., & Loken, C. 1996, ApJ, 473, 651
Roettiger, K., Loken, C., & Burns, J. O. 1997, ApJS, 109, 307
Roettiger, K., Burns, J. O., & Stone, J. M. 1999, ApJ, 518, 603
Russell, H. R., van Weeren, R. J., Edge, A. C., et al. 2011, MNRAS, 417, L1
Sarazin, C. L. 2002, in Merging Processes in Galaxy Clusters, ed. L. Feretti, I. M. Gioia, & G. Giovannini (The Netherlands: Kluwer Ac. Pub.), 1
Schuecker, P., Böhringer, H., Reiprich, T. H., & Feretti, L. 2001, A&A, 378, 408
Serna, A., & Gerbal, D. 1996, A&A, 309, 65
Skillman, S. W., Hallman, E. J., O'Shea, B. W., et al. 2011, ApJ, 735, 96
Struble, M. F., & Rood, H. J. 1987, ApJS, 63, 555
Thompson, L. A. 1982, in Early Evolution of the Universe and the Present Structure, ed. G. O. Abell, & G. Chincarini (Dordrecht: Reidel), IAU Symp., 104
Tonry, J., & Davis, M. 1979, ApJ, 84, 1511
Tribble, P. C. 1993, MNRAS, 261, 57
Venturi, T., Giacintucci, S., Macario, G., et al. 2008, A&A, 484, 327
Wainer, H., & Schacht, S. 1978, Psychometrika, 43, 203
West, M. J., & Bothun, G. D. 1990, ApJ, 350, 36